International Journal of Climatology

International Journal of Climatology RMetS

RESEARCH ARTICLE

Future Climate Changes on the Qinghai–Tibetan Plateau Under CMIP6 Global Climate Models

Rizwan Karim[1,2] | Shufeng Li[1,3] | Tao Su[1,3,4] | Brian Odhiambo Ayugi[5] | Hassen Babaousmail[6] | Shumei Xiao[1,3]

[1]CAS Key Laboratory of Tropical Forest Ecology, Xishuangbanna Tropical Botanical Garden, Chinese Academy of Sciences, Mengla, Yunnan, People's Republic of China | [2]School of Earth Sciences, Yunnan University, Kunming, People's Republic of China | [3]University of Chinese Academy of Sciences, Beijing, People's Republic of China | [4]State Key Laboratory of Oil and Gas Reservoir Geology and Exploitation & Institute of Sedimentary Geology, Chengdu University of Technology, Chengdu, People's Republic of China | [5]Faculty of Civil Engineering, Seoul National University of Science and Technology, Seoul, South Korea | [6]School of Atmospheric Science and Remote Sensing, Wuxi University, Wuxi, People's Republic of China

Correspondence: Rizwan Karim (rizwan@xtbg.ac.cn)

Received: 18 July 2024 | **Revised:** 5 June 2025 | **Accepted:** 6 June 2025

Funding: This study was supported by Postdoctoral research funding of Xishuangbanna Tropical Botanical Garden-CAS, the Young and Middle-aged Academic and Technical Leaders of Yunnan (no. 202305AC160051) and the 14th Five-Year Plan of the Xishuangbanna Tropical Botanical Garden, Chinese Academy of Sciences (E3ZKFF1K, E3ZKFF7B).

Keywords: CMIP6 | global climate models | precipitation | projections | Qinghai–Tibetan plateau | temperature

ABSTRACT

Rapid climate change on the Qinghai-Tibetan Plateau (QTP) is reshaping ecosystems, altering water availability and affecting human livelihoods. Understanding the timing and distribution of these changes is now critical. This study examines precipitation and temperature changes from 1980 to 2100 using CMIP6 global climate models (GCMs) and high-resolution observational data. It examined seasonal and annual variability, model biases and projected changes for various climate scenarios. Our findings show that climate models consistently overestimated precipitation, particularly in southeastern QTP, while cold biases are prevalent in central and western regions in the past. Seasonal precipitation patterns exhibit significant variation across QTP. Bias corrections enhanced model reliability, reinforcing projections of wetter conditions and continued warming across QTP. Future projections indicate wetter conditions in winter and summer, though some areas may experience a slight decline in annual accumulations. Temperature trends project pronounced warming across all seasons, with the strongest increases expected in winter. Both maximum and minimum temperatures project significant upward trends, particularly at higher elevations. These findings indicate a shift toward a warmer and wetter climate at QTP, with potential environmental and socio-economic impacts. The study underscores the urgency of adaptive strategies to mitigate climate risks and enhance resilience in this high-altitude environment.

1 | Introduction

The Qinghai–Tibetan Plateau (QTP), often referred to as the "Roof of the World," is an essential area for studying climate change because of its great elevation, intricate topography and its role in influencing both regional and global atmospheric circulation (Zhang, You, et al. 2022; Yao et al. 2019; Zhang, Liu, et al. 2022). The QTP is critical in regulating monsoon patterns, hydrological cycles and the cryosphere, as it is the source of major river systems such as the Yangtze, Yellow, Mekong and Brahmaputra Rivers, which provide water to over 1.4 billion people downstream (Zhang, You, et al. 2022).

In the past 50 years, the QTP has experienced warming at nearly double the global average rate, resulting in accelerated glacier melting, permafrost thawing and instability in ecosystems

(Zhang, You, et al. 2022). Despite the extensive research on climate variability in the QTP, significant uncertainties persist regarding the spatial and temporal changes in temperature and precipitation, especially at varying elevations and across different seasons (Chen et al. 2020; Cui et al. 2021; Ayugi et al. 2020; Ngoma et al. 2021; Fan et al. 2022; Zhang, You, et al. 2022; Lun et al. 2021).

Numerous studies have analysed past and projected temperature and precipitation trends on the QTP using datasets from the Coupled Model Intercomparison Project Phase 5 (CMIP5) and Phase 6 (CMIP6) (Hu et al. 2014; You, Jiang, et al. 2016; Xu, Zhang, et al. 2016). While CMIP5 models have successfully captured large-scale temperature patterns, they have inherent biases, particularly cold biases for temperature simulations and wet biases for precipitation estimates, especially in high-altitude areas (Ayugi et al. 2020; Ngoma et al. 2021; Fan et al. 2022; Zhang, You, et al. 2022; Lun et al. 2021; Cui et al. 2021). The newer CMIP6 models show advancements in spatial resolution, cloud parameterization and representation of radiative forcing, yet they still carry uncertainties regarding extreme temperature occurrences and variations in precipitation forecasts (Fan et al. 2022; Zhang, You, et al. 2022; Zhou et al. 2023; Zhang, Liu, et al. 2022). Projections suggest that surface air temperature over the QTP could rise by 3°C–7°C by the end of the 21st century under SSP5-8.5 scenarios, with maximum (*tmax*) and minimum (*tmin*) temperatures increasing at a rate between 0.19°C and 0.36°C per decade (You et al. 2017; Zhang, You, et al. 2022). Despite these predictions, the extent, geographical distribution and elevation-related dependence of these changes remain uncertain, emphasising the need for further high-resolution climate modelling research (Zhang, You, et al. 2022).

A key factor influencing future warming in the QTP is Elevation-Dependent Warming (EDW), which indicates that regions at higher altitudes experience substantially greater temperature increases (You, Chen, et al. 2020; Zhang, You, et al. 2022). Several mechanisms contribute to EDW, including rises in atmospheric moisture content, improved absorption of solar radiation and feedback loops related to snow and glacier reduction (You, Chen, et al. 2020; Zhang, You, et al. 2022). Although there is strong observational evidence supporting EDW, General Circulation Models (GCMs) struggle to accurately represent its magnitude and regional variability, resulting in significant biases in future climate estimates (Zhang, You, et al. 2022). Additionally, uncertainties regarding variations in *tmax* and *tmin* create notable limitations, hindering our capacity to forecast heatwave magnitudes, frost occurrences and daily temperature variations (Chen et al. 2017). Addressing these uncertainties is crucial for enhancing climate predictions and delivering more precise evaluations of extreme temperature events in the QTP.

In addition to temperature biases, precipitation forecasts for the QTP remain exceedingly uncertain, with pronounced seasonal and regional differences. Historical data show a slight rise in precipitation since the 1960s, although this trend displays considerable spatial and temporal variability (Xu et al. 2007; Zhang, You, et al. 2022). Both CMIP5 and CMIP6 models often overpredict precipitation levels, particularly in regions influenced by monsoon activity, due to their inability to comprehensively represent convective processes and atmospheric moisture transport dynamics (Ayugi et al. 2020; Ngoma et al. 2021; Fan et al. 2022; Zhang, You, et al. 2022; Lun et al. 2021; Cui et al. 2021). Future precipitation forecasts are highly inconsistent, with some research indicating wetter summers and drier winters, while other studies propose a general increase in annual precipitation (Fan et al. 2022; Zhang, You, et al. 2022). These discrepancies highlight the importance of robust bias correction methods to enhance the accuracy of climate models and guide critical policy decisions related to water resources, agriculture and climate adaptation strategies.

Bias correction techniques have been commonly utilised in climate modelling to mitigate systematic errors in Global Climate Model (GCM) outputs (Ayugi et al. 2020; Ngoma et al. 2021; Fan et al. 2022; Zhang, You, et al. 2022). One of the most effective methods for adjusting modelled climate variables to align with observed data and correct systematic biases is Quantile Mapping Bias Correction (QMBC) (Gudmundsson et al. 2012; Ayugi et al. 2020; Ngoma et al. 2021; Jose and Dwarakish 2022). QMBC has proven to significantly enhance the downscaling of temperature and precipitation projections, particularly in high-altitude regions (Ayugi et al. 2020; Fan et al. 2022; Zhang, You, et al. 2022). Despite its prevalent application, there are concerns about the potential inflation of variability due to quantile-based adjustments (Maraun 2013). Some research indicates that QMBC could inadvertently exaggerate extreme temperature and precipitation events, highlighting the need for further refinement and assessment in high-mountain areas such as the Tibetan Plateau (QTP) (Maraun 2013; Gudmundsson et al. 2012). Given these issues, there have been limited systematic applications of QMBC to CMIP6 projections over the QTP, resulting in a significant gap in bias-corrected climate datasets (Ayugi et al. 2020; Ngoma et al. 2021; Fan et al. 2022; Zhang, You, et al. 2022). Addressing this gap is essential for enhancing regional climate adaptation strategies and hydrological impact evaluations.

The goal of this study is to assess biases in CMIP6 models and produce bias-corrected projections for precipitation, maximum temperature (*tmax*), minimum temperature (*tmin*) and average temperature (*tas*) across winter, summer and annual timescales in the QTP. By implementing QMBC, this research aims to improve the reliability of future climate projections, providing critical insights for policymakers, water resource managers and climate adaptation planning. In contrast to prior studies, this research specifically investigates spatial and temporal trends across multiple Shared Socioeconomic Pathways (SSP) scenarios (SSP2-4.5 and SSP5-8.5), delivering a comprehensive, high-resolution evaluation of future climate variability within the QTP.

The remainder of this paper is organised as follows: Section 2 details the datasets, GCMs and statistical methodologies utilised, including bias correction techniques. Section 3 presents the results, while Section 4 discusses their implications. Finally, Section 5 concludes with suggestions for future research, climate adaptation strategies and improvements in GCM-based climate projections.

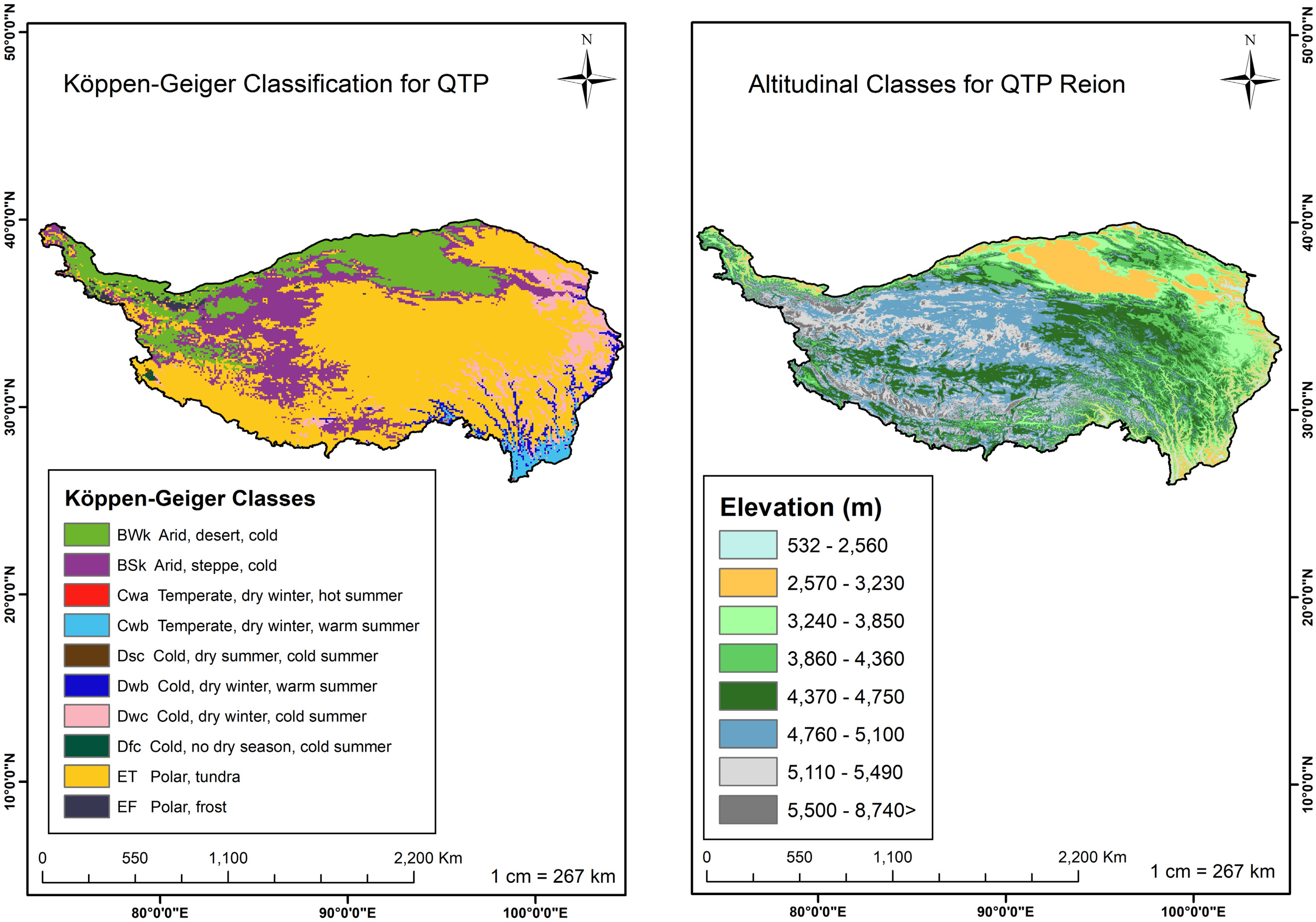

FIGURE 1 | The distribution of elevation and land cover features across the Qinghai–Tibetan Plateau region (Zhang et al. 2021). [Colour figure can be viewed at wileyonlinelibrary.com]

2 | Study Area, Data and Methodology

2.1 | Study Area

The QTP is located in Asia, spanning 23° N–40° N and 73° E–106° E (Figure 1). It is flanked by the Qilian and Kunlun Mountains to the north, the Himalayan Mountains to the south, the Karakorum Range to the west and the Hengduan Mountains to the east. As the world's highest and largest plateau, it averages an elevation of 4000 m and covers roughly 2.5 million square kilometres (Zhang et al. 2021). The plateau generally transitions from warm and humid in the southeast to cold and dry in the northwest. Its annual average air temperature is below 0°C, with the highest temperatures reaching up to 10°C (Feng et al. 2020). Precipitation distribution on the Tibetan Plateau (TP) is highly uneven, with most rainfall occurring from May to September during the rainy season. In areas with relatively high precipitation, the rainy season accounts for 60%–70% of the annual total, while in drier regions, it constitutes 80%–90% of the yearly rainfall (Li et al. 2017; Xu, Zhang, et al. 2016).

The QTP has experienced rising annual temperatures, particularly between 1955 and 1996, at a rate of 0.16°C per decade for winter temperatures, making it highly sensitive to global climate change (Kuang and Jiao 2016). Since the 1950s, there has been a slight increase in precipitation, though rainfall pattern changes vary across the region.

2.2 | CMIP6 GCM Outputs and CN05.1 Datasets

In this study, we downloaded and processed daily gridded CN05.1 datasets from the National Meteorological Information Center, China Meteorological Administration (Wu and Xue-Jie 2013) to analyse precipitation, *tas*, *tmax* and *tmin* variables for the period 1980–2014. The CN05.1 dataset (0.25° resolution) integrates over 2400 stations across China, including 300–500 in the QTP, providing a superior benchmark for regional climate variability. We also downloaded and processed daily outputs from 18 CMIP6 models (r1i1p1f1) from the CMIP6 repository (https://esgf-node.llnl.gov/search/cmip6) to analyse climate variables over the QTP from 1980 to 2100 (Table S1). These models were chosen to accommodate the study's extensive variable set precipitation, *tas*, *tmax* and *tmin* and their in-depth analysis. The number of models in an ensemble and its size depend on the specific application or research question, with no clear consensus on the optimal size (Lu et al. 2022; Maher et al. 2018; Ullah et al. 2022). The future scenarios (2015–2100) of SSP2-4.5 and SSP5-8.5 were chosen to examine their evolution as response to future GHG emissions.

All the downloaded CMIP6 datasets were standardised to ensure consistency in units and calendar time. The GCMs and CN05.1 dataset were regridded to a 1° × 1° resolution using the bilinear interpolation method. To reduce future biases and distinguish external forcing from internal variability, multi-model ensembles (MMEs) were created for the historical period and all SSP scenarios, following the technique recommended by Milinski et al. (2019) and Ullah et al. (2022). Winter, summer and annual values of the four variables were calculated for historical datasets and future bias-corrected scenarios.

2.3 | Methodology

2.3.1 | Spatio-Temporal Simulations

The winter (December–January–February), summer (June–July–August) and annual (January–December) simulations from 1980 to 2014 were calculated for the variables to observe patterns and evaluate the seasonal performance of all GCMs. The temporal evolution of all variables during this period was also determined. The Mann–Kendall (MK) test was used to investigate the temporal trend and assess its significance for precipitation, *tas*, *tmax* and *tmin* across all time scales, with a significance level of 5%. The MK trend test can handle outliers and missing values and does not require datasets to follow a normal distribution (Mann 1945; Kendall 1975). A similar approach has been employed in other similar related studies across various regions (Lu et al. 2022; Ullah et al. 2022; Ayugi et al. 2024). The results are described in the Supporting Information in detail.

2.3.2 | Model Performance Metrics

The evaluation used statistical metrics of bias, root mean square error (RMSE) and correlation coefficient (*r*). Further details on these statistics can be found in the works of Karim et al. (2020, 2023) and Ngoma et al. (2021). The historical spatial bias of the MMEs for seasonal and annual precipitation, *tas*, *tmax* and *tmin* was assessed. The statistical formulas for the metrics are:

$$\text{Bias} = \frac{1}{N}\sum_{k=1}^{N}(Mi - Oi) \tag{1}$$

$$\text{RMSE} = \sqrt{\frac{1}{N}\sum_{k=1}^{N}(Mi-Oi)^2} \tag{2}$$

$$r = \frac{\sum_{k=1}^{n}\left(Oi-\overline{Oi}\right)\left(Mi-\overline{Mi}\right)}{\sqrt{\sum_{k=1}^{n}\left(Oi-\overline{Oi}\right)^2\sum_{k=1}^{n}\left(Mi-\overline{OMi}\right)^2}} \tag{3}$$

where *M* is model simulated and *O* is observed variable values, *i* denote observed and simulated pairs while n shows total number of pairs.

Taylor diagrams were used to measure the agreement between models and observations, considering climatology patterns. This was done using correlation coefficients, RMSE and the ratio of standard deviations (Taylor 2001). The Taylor Skill Score (TSS) ranks the GCMs based on their performance, considering standard deviation and correlation coefficients (Taylor 2001). Implementation of Taylor metrics can be found in the works of Ayugi et al. (2021) and Babaousmail et al. (2021):

$$\text{TSS} = \frac{4\left(1+R_m\right)^2}{\left(\frac{\sigma_m}{\sigma_o}+\frac{\sigma_o}{\sigma_m}\right)^2\left(1+R_o\right)^2} \tag{4}$$

where, R_m is the spatial correlation coefficient for simulated and observed variable patterns, R_o is the full attainable correlation coefficient (i.e., 0.999), while σ_m and σ_o are the standard deviations of simulated and observed temperature patterns, respectively. The TSS value ranges from 0 to 1, with values closer to 1 indicating better model performance. The results are described in Supporting Information in detail.

2.3.3 | Bias Correction

Persistent biases in CMIP6 GCMs for climatic variables over the QTP region (Zhou and Zhang 2021; Zhang, Liu, et al. 2022) necessitate an effective bias reduction method to obtain reliable future projections. QMBC is a straightforward and efficient technique with low computational demands, successfully applied to various variables in regions such as the Horn of Africa (Ayugi et al. 2020), South Asia (Gupta et al. 2019) and Europe (Cardell et al. 2019). QMBC aligns the model's cumulative density function (CDF) distribution with the observed distribution, ensuring that the model's output matches the observed data while maintaining rank correlation.

For normally distributed temperature variables, the QMBC method can be expressed as follows (Gupta et al. 2019):

$$X^{-}_{ms.corr} = +F^{-1}_{oh}\left(F_{ms}\left(X_{ms}\right)\right) - F^{-1}_{mh}\left(F_{ms}\left(X_{ms}\right)\right) \tag{5}$$

For precipitation, which often follows a gamma distribution, the corrected model simulation is given by:

$$X^{-}_{ms.corr} = \begin{cases} F^{-1}_{oh}\left(F_{ms}\left(X_{ms}\right)\right), & if\, xms \geq xth \\ 0, & if\, xms \leq xth \end{cases} \tag{6}$$

where *X* is a climatic variable, *Xms.corr* is bias-corrected model simulated data; *F* is CDF, whereas F^{-1} is its inverse. (o = observed, m = model, h = historical period and s = simulation/projection period). This study applied QMBC to initially bias-correct monthly variables of precipitation, *tas*, *tmax* and *tmin* for the historical period 1980–2014. The QMBC method was implemented in the Climate Data Bias Correction tool (Gupta et al. 2019) by first calculating bias coefficients for 1980–2014 and then incorporating them into raw historical and future GCM scenarios of SSP2–4.5 and SSP5–8.5. The results are provided in detail in Supporting Information in detail.

2.3.4 | QMBC Performance Evaluation for GCMs

To assess the response of selected GCMs to the implementation of the QMBC approach, we conducted a probability density function (PDF) analysis. This analysis was performed to compare changes in bias-corrected simulation values before and after correction against the benchmark dataset CN05.1. The PDF analysis employs an integral function for continuous random variables across multiple intervals, allowing us to determine the probability of occurrence for various values within those intervals (Ali et al. 2021). In this study, we utilised kernel smoothing density estimation, which helps identify and categorise likely changes as well as rare events (Farooqui and Soomro 1984).

2.3.5 | Bias-Corrected Future Climate Projections

This study analyses future climate changes in seasonal and annual precipitation, near-surface air temperature (*tas*), maximum temperature (*tmax*) and minimum temperature (*tmin*) under SSP2-4.5 and SSP5-8.5 scenarios for the period from 2015 to 2100, utilising bias-corrected projections. Changes were quantified by comparing future climate values to a historical baseline (1980–2014). Probabilistic estimates, including means and ranges, were used to capture uncertainties and provide a clearer understanding of warming trends and precipitation variability (Brunner et al. 2020).

Future climate conditions were evaluated for mid-century (2023–2056) and late-century (2067–2100) timescales by comparing projected anomalies with historical trends. Research indicates that 20-, 25- and 30-year timeframes yield spatially consistent and statistically significant trends ($p < 0.05$), effectively balancing interannual variability and anthropogenic climate change signals (You et al. 2021; Hawkins et al. 2020). The IRLS regression method was used to analyse spatial trends, ensuring outlier robustness, crucial for high-altitude regions like the QTP (Iyakaremye et al. 2021). This study offers key insights for climate adaptation, water resource management and extreme event analysis over the QTP.

3 | Results

3.1 | Historical Climate Simulations and Persistent Biases

The evaluation of historical seasonal and annual precipitation and temperature simulations (*tas*, *tmax*, *tmin*) from 1980 to 2014 reveals substantial discrepancies between observed data and the MME (Figure 2). Precipitation simulations consistently overestimate values, particularly in summer, with observed precipitation ranging from 240 to 340 mm/year, while MME estimates fluctuate between 470 and 520 mm/year. Annual precipitation figures are documented between 440 and 550 mm/year, in stark contrast to MME projections of 960 to 1065 mm/year. Seasonal bias distribution indicates wet biases of 0–350 mm in summer and 0 to 140 mm in winter for the southern QTP, with annual precipitation bias peaking at 1100 mm in the southeast (Figure 2). Trends in Table S2 show significant increases in annual (0.43 to 0.46 mm/year) and summer precipitation (0.27 to 0.32 mm/year).

Winter *tas* from 1980 to 2014 reveal lower values in observed data (−12.8°C to −11.7°C) compared to MME data (−11.6°C to −8.1°C) (Figure 2), while summer *tas* continuously increased in observed data (8.6°C to 10.3°C) and MME (8.6°C to 10.1°C). Notably, the MME consistently underestimated observed *tas* values across all timeframes. The trends (Table S2) record significant warming in the winter (0.02°C/year), annual (0.06°C/year) and summer season (0.03°C/year). MME trends reflect the observed patterns, even if they are modest in size. Temperature simulations exhibit seasonal biases, with winter *tas* underestimated (observed: −12.8°C to −11.7°C; MME: −11.6°C to −8.1°C) and summer *tas* values slightly underrepresented (observed: 8.6°C–10.3°C; MME: 8.6°C–10.1°C). Bias analysis highlights significant cold biases in winter *tas* (−12°C to 0°C) and moderate cold biases in summer *tas* (−6°C to 0°C) in the south (Figure 2). The annual *tas* distribution shows cold biases (−4°C to 0°C) with warm biases in the northeast. It is observed that CMIP6 advancements simulate reduced northwest QTP cold biases to about 1°C compared to CMIP5 GCMs (Lun et al. 2021).

Winter *tmax* shows observed values from −4.3°C to 0.1°C, while MME values range from −7.6°C to 5.4°C, maintaining underestimation (Figure 3). The Biases analyses show cold biases for winter *tmax* (−6°C to 0°C) and *tmin* (−11°C to 0°C) (Figure 3). The observed trends in *tmax* during winters exhibit the most substantial changes at 0.09°C/year, followed by 0.03°C/year in summers and 0.06°C/year annually (Table S4). The MME trends, although small in magnitude, align with these patterns for seasonal and annual *tmax*.

Similarly, winter *tmin* values (Figure 3) portray an increase across the QTP in observed data (ranging from −18.3°C to −15.5°C) and in the MME data (ranging from −18.7°C to −17.1°C) with persistent cold biases (−11°C to 0°C) for the season. Likewise, summer *tmin* values also demonstrate a notable increase in observed data (ranging from 3.2°C to 5.4°C) and in MME data (ranging from 3.7°C to 5.6°C) over the QTP. It is noteworthy that the MME underestimates observed *tmin* values in summer and overestimates them in winter and annually. Annual *tmin* values also depict an increase in observed data (ranging from −6.6°C to −4.7°C) and in MME data (ranging from −6.8°C to −5.5°C). The observed trends (Table S5) for *tmin* are particularly robust in winters at 0.07°C/year, followed by summers at 0.01°C/year, and annually at 0.02°C/year. The MMEs depict the strongest trend during winters, followed by annual and summer timescales. Trends across all temperature variables indicate significant warming especially in winters. The warming is most pronounced during winter, attributed to solar activity variations and while precipitation changes could be attributed to the large-scale air-sea interactions (Haigh 1996; Meehl et al. 2008). Importantly, the overestimations in precipitation while underestimating winter temperature extremes, reflects the ongoing challenges in modelling snow-ice feedbacks and regional variability (Jiang et al. 2005, 2016; You et al. 2019).

3.2 | Twenty-First Century Climate Change Projections

3.2.1 | Projected Changes in Precipitation

Following the successful application of bias correction, the study investigated potential changes in climatic variables under the MME for both modest mitigation (SSP2–4.5) and business-as-usual (SSP5–8.5) pathways throughout the mid (2023–2056), late (2067–2100) and entire 21st century. Figure 4 depicts changes in winter, summer and annual precipitation and *tas* over the QTP. Winter precipitation is

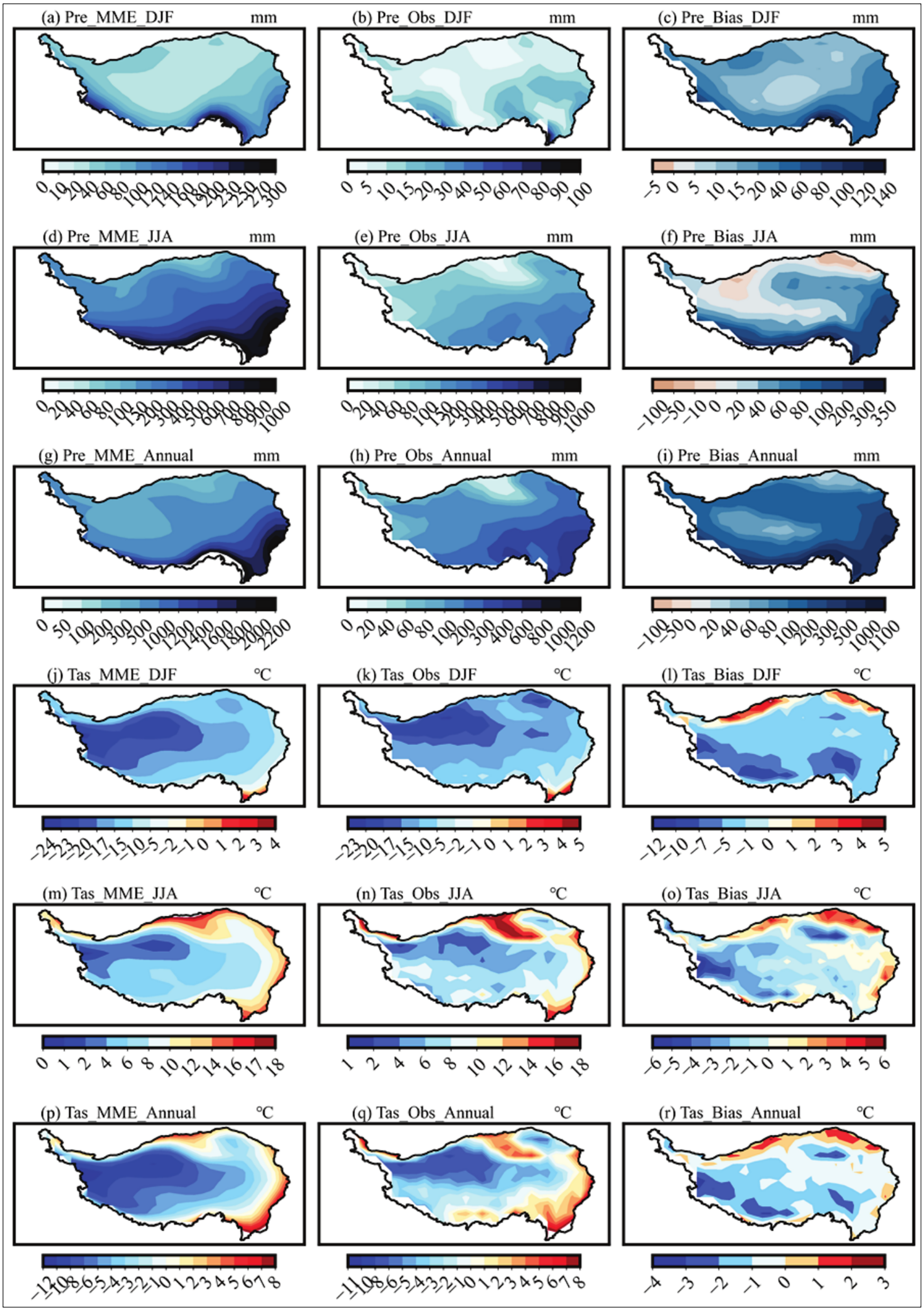

FIGURE 2 | The winter, summer and annual spatial distribution of observed (b, e, h) and MME precipitation (a, d, g), observed (k, n, q) and MME (j, m, p) data delineated the *tas* variable for 1980–2014 across the QTP region. The rightmost column shows the seasonal and annual biases in the precipitation (c, f, i) and *tas* (l, o, r) for all three timescales. Precipitation shows stronger magnitudes at the southern and southeastern regions, whereas *tas* shows stronger magnitudes at the northern and northeastern areas for the mentioned years. [Colour figure can be viewed at wileyonlinelibrary.com]

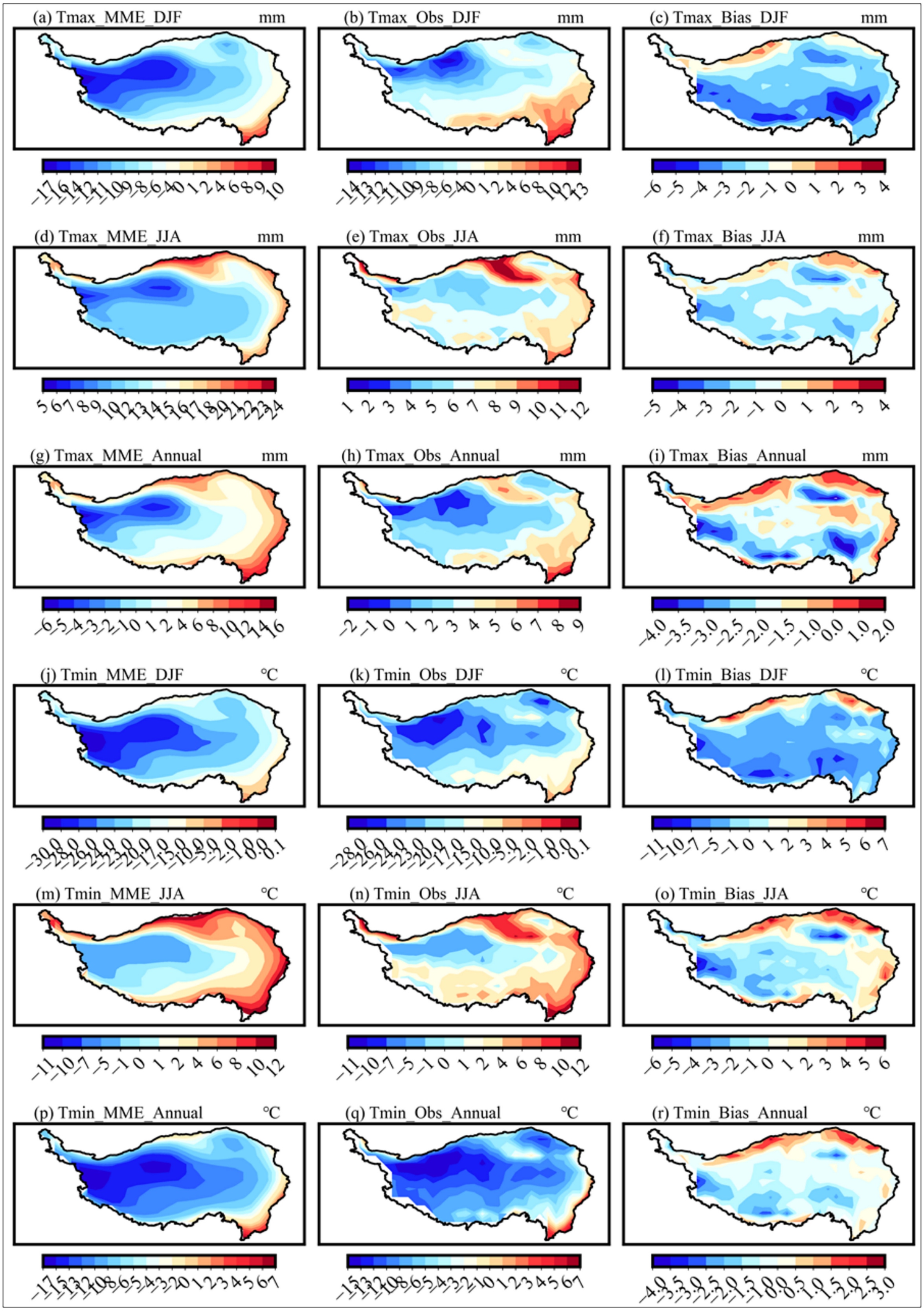

FIGURE 3 | The spatial distributions of winter, summer and annual maximum (*tasmax*) and minimum (*tasmin*) temperatures from 1980 to 2014 over the Qinghai–Tibetan Plateau (QTP) are shown using both observations and multi-model ensemble (MME) outputs. Panels (a, d, g) and (b, e, h) represent *tasmax* from MME and observations, respectively, while panels (j, m, p) and (k, n, q) show the same for *tasmin*. The rightmost column (c, f, i for *tasmax*; l, o, r for *tasmin*) illustrates seasonal and annual biases across the datasets. Both *tasmax* and *tasmin* exhibit higher values primarily in the eastern region with pronounced values in the northern and northeastern regions. [Colour figure can be viewed at wileyonlinelibrary.com]

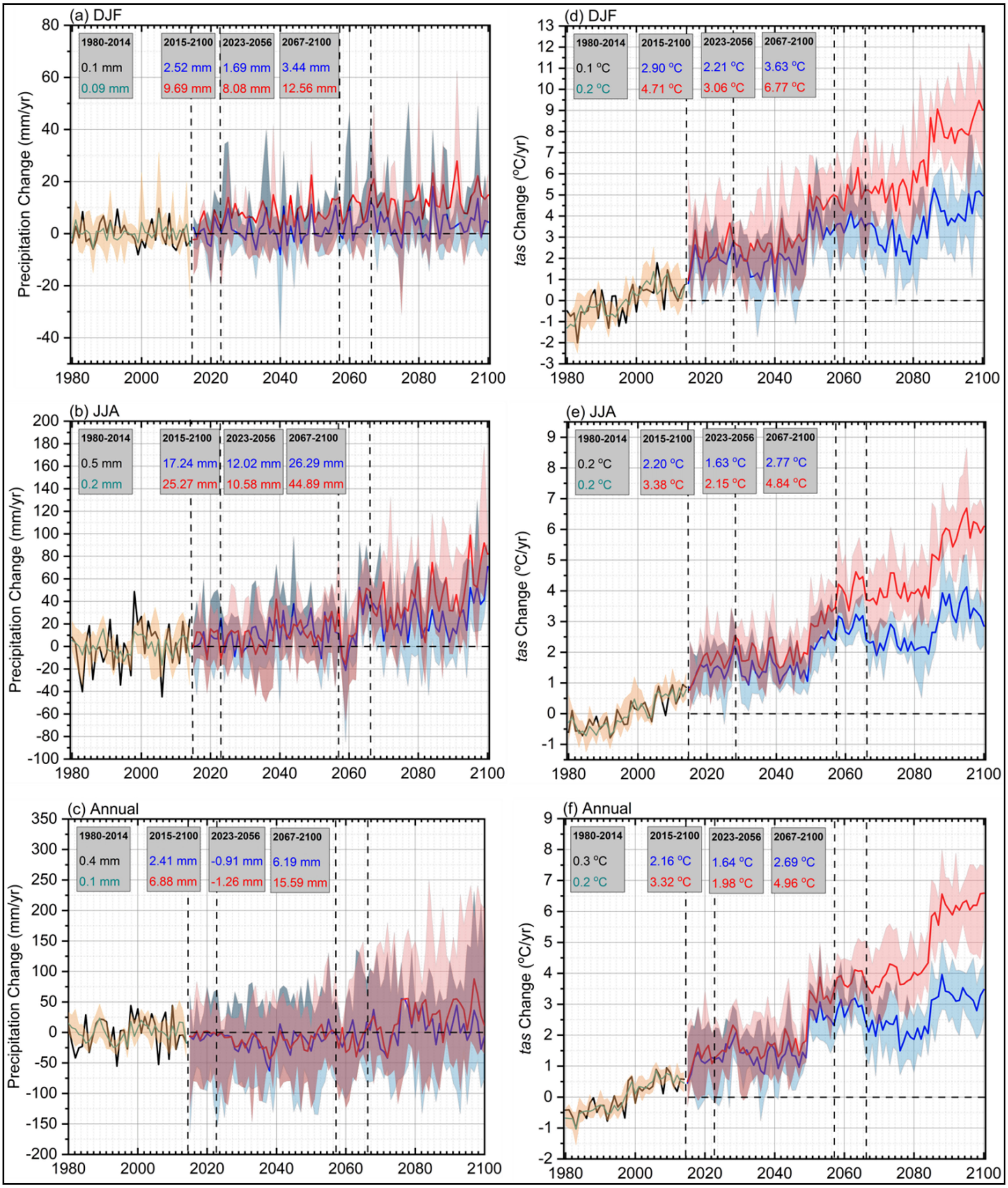

FIGURE 4 | Projected changes in bias-corrected multi-model ensemble (MME) outputs for seasonal and annual precipitation (a–c) and near-surface air temperature (*tas*; d–f) over the Qinghai–Tibetan Plateau (QTP) under SSP2-4.5 (blue line) and SSP5-8.5 (red line), relative to the 1980–2014 baseline (olive green line). The black line represents observed values. Shaded areas—orange for historical, light blue for SSP2-4.5 and pink/red for SSP5-8.5—indicate the inter-model spread. Vertical dashed lines divide the future into three time slices: 2015–2100, 2023–2056 and 2067–2100. Mean changes during these periods are summarised in grey-shaded insets, with values shown in green (historical), blue (SSP2-4.5) and red (SSP5-8.5) text. Results highlight stronger warming and precipitation increases under the high-emissions SSP5-8.5 scenario, particularly in the latter half of the century. [Colour figure can be viewed at wileyonlinelibrary.com]

TABLE 1 | Mean and Mann–Kendall trend values of precipitation, *tas*, *tmax* and *tmin* variables over QTP region during 21st century, mid-century and late century periods under the SSP2–4.5 and SSP5–8.5 scenarios based on bias corrected MME of CMIP6 GCMs.

Season	scenario	2015–2100 Mean	2015–2100 MK trend	2015–2100 Trend sign	2023–2056 Mean	2023–2056 MK trend	2023–2056 Trend sign	2067–2100 Mean	2067–2100 MK trend	2067–2100 Trend sign
(Pre) Winter	SSP2–4.5	20.52	0.29	▲=	19.66	0.176	▲≠	21.43	0.159	▲≠
	SSP5–8.5	21.01	<0.000	▲=	19.43	0.178	▲≠	23.48	0.207	▲≠
(Pre) Summer	SSP2–4.5	194.99	<0.000	▲=	190.08	0.228	▲≠	204.44	0.226	▲≠
	SSP5–8.5	223.60	0.200	▲=	208.86	0.132	▲=	243.95	0.343	▲=
(Pre) Annual	SSP2–4.5	358.79	0.061	▲=	348.98	0.206	▲=	374.49	0.201	▲≠
	SSP5–8.5	371.19	0.010	▲=	347.04	0.005	▲=	403.37	0.293	▲=
(*tas*) Winter	SSP2–4.5	−9.1	0.11	▲=	−9.7	<0.000	▲=	−8.3	0.20	▲=
	SSP5–8.5	−7.3	0.20	▲=	−8.8	0.18	▲=	−5.1	0.25	▲=
(*tas*) Summer	SSP2–4.5	9.9	0.03	▲=	9.4	<0.000	▲=	10.6	0.05	▲=
	SSP5–8.5	11.1	0.04	▲=	10.0	0.096	▲=	12.6	0.19	▲=
(*tas*) Annual	SSP2–4.5	0.3	0.01	▲=	−0.1	<0.000	▲=	1.0	0.18	▲=
	SSP5–8.5	1.5	0.02	▲=	0.3	0.20	▲=	3.2	0.21	▲=
(*tmax*) Winter	SSP2–4.5	−1.0	0.200	▲=	−1.5	0.04	▲=	−0.3	0.14	▲=
	SSP5–8.5	0.3	0.300	▲=	−1.2	0.13	▲=	2.3	0.17	▲=
(*tmax*) Summer	SSP2–4.5	16.6	0.162	▲=	16.0	0.01	▲=	17.3	0.09	▲=
	SSP5–8.5	17.8	0.171	▲=	16.5	0.17	▲=	19.6	0.24	▲=
(*tmax*) Annual	SSP2–4.5	8.0	0.074	▲=	7.5	0.013	▲=	8.7	0.03	▲=
	SSP5–8.5	9.2	0.082	▲=	7.9	0.13	▲=	11.2	0.09	▲=
(*tmin*) Winter	SSP2–4.5	−15.9	0.33	▲=	−16.4	0.21	▲=	−15.2	0.17	▲≠
	SSP5–8.5	−14.7	0.42	▲=	−16.1	0.33	▲=	−12.8	0.58	▲=
(*tmin*) Summer	SSP2–4.5	4.5	0.15	▲=	4.1	0.030	▲=	5.2	0.18	▲=
	SSP5–8.5	5.7	0.21	▲=	4.5	0.120	▲=	7.4	0.22	▲=
(*tmin*) Annual	SSP2–4.5	−5.6	0.20	▲=	−6.1	0.040	▲=	−4.9	0.16	▲=
	SSP5–8.5	−4.2	0.30	▲=	−5.6	0.200	▲=	−2.1	0.36	▲=

Note: The value <0.000 represents the trend values smaller than 0.0001. The ▲/▼ signs indicate increase/decrease in the trend. The = and ≠ denotes significant and insignificant trend at 95% confidence interval.

expected to rise by an average of 2.5 mm/year (SSP2–4.5) and 10 mm/year (SSP5–8.5) in the 21st century, with late-century values reaching 3.4 mm/year (SSP2–4.5) and 13 mm/year (SSP5–8.5). Summer precipitation is projected to increase by 17.4 mm/year (SSP2–4.5) and 25.3 mm/year (SSP5–8.5), with late-century values reaching 26 mm/year (SSP2–4.5) and 44 mm/year (SSP5–8.5). Annual precipitation shows an increasing pattern, ranging from −2.41 mm/year (SSP2–4.5) to 6.68 mm/year (SSP5–8.5). Mid-century projections show a decrease of −0.91 mm (SSP2–4.5) and −1.26 mm (SSP5–8.5), while end-of-century projections show increases of 6.19 mm/year (SSP2–4.5) and 15.59 mm/year (SSP5–8.5). Projection uncertainties are notably lower for winter, summer and annual timescales, as reflected by the relatively narrow inter-model spread. Corresponding precipitation trends (Table 1) further substantiate these findings, with pronounced increases projected for late-century summer (0.343 mm/year) and annual precipitation (0.293 mm/year) under the SSP5–8.5 scenario. These changes are further supported by box-and-whisker plots (Figure S20a–c), which illustrate statistically significant precipitation increases, particularly during mid- and late-century summers in the high-emission pathway.

Figure 5 depicts the spatial distribution of trends in winter, summer and annual precipitation using the IRLS method for the twenty-first century. Winter precipitation (Figure 5a–f) is projected to increase across the southeastern QTP under SSP2–4.5 (0.01–0.05 mm/year) and SSP5–8.5 (0.01–0.10 mm/year), with a more robust increase in the late century (0.01–0.12 mm/year). Summer precipitation (Figure 5g–l) is expected to rise in parts of southern QTP under SSP2–4.5 (0.01–0.10 mm/year) and SSP5–8.5 (0–0.13 mm/year), while negative tendencies (−0.01

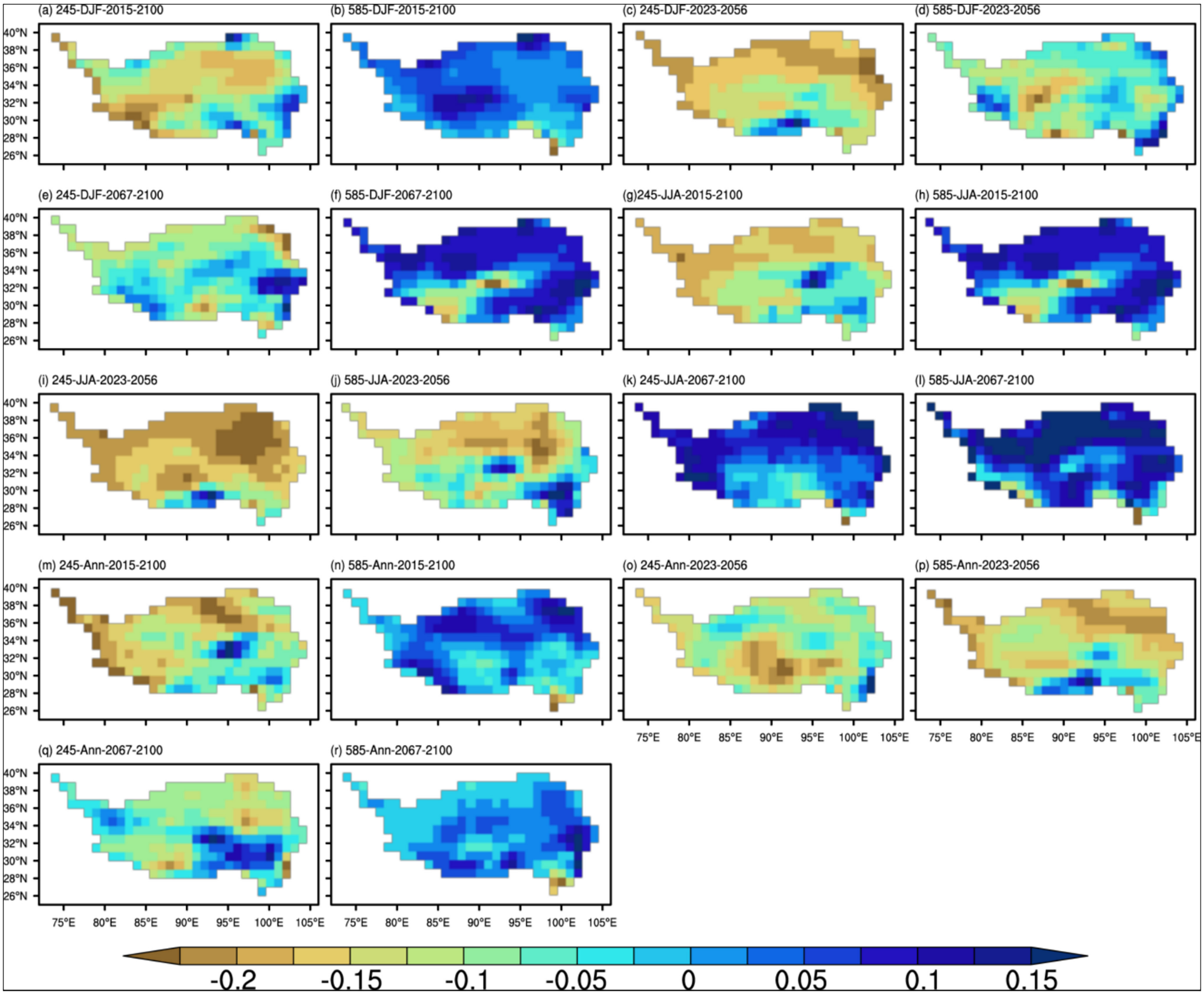

FIGURE 5 | Spatial distribution of projected precipitation change trends (mm/year) over the Qinghai–Tibetan Plateau (QTP) under SSP2-4.5 and SSP5-8.5 scenarios for three future periods: 2015–2100, 2023–2056 and 2067–2100. Panels (a–f) show changes for winter (DJF), (g–l) for summer (JJA) and (m–r) for annual scales. The left column in each pair represents SSP2-4.5 and the right represents SSP5-8.5. Colour gradients range from drying (brown) to wetting (blue), with scale units in mm/year. SSP5-8.5 projects stronger and more widespread increases in precipitation, particularly in summer and in the central and southeastern regions of the QTP. SSP2-4.5 shows more moderate or regionally varied changes. [Colour figure can be viewed at wileyonlinelibrary.com]

to −0.13 mm/year) elsewhere. Late-century projections show more significant increases, particularly under SSP5-8.5 (0.01 to 0.15 mm/year). Annual precipitation (Figure 5m–r) is projected to increase across the southeastern QTP under SSP2–4.5 (0.01–0.10 mm/year) and across the entire QTP under SSP5–8.5 (0.01–0.14 mm/year). Southern to southeastern parts are likely to experience increased precipitation in the late century under both SSP2–4.5 (0.01–0.10 mm/year) and SSP5–8.5 (0.01–0.15 mm/year). Overall, summer, annual and winter precipitation are expected to rise, particularly under SSP5–8.5.

3.2.2 | Projected Changes in Mean Temperature (*tas*)

Figure 4d–f depicts changes in winter, summer and annual precipitation and *tas* over the QTP. Winter temperatures are projected to increase by 2.9°C and 4.7°C in the 21st century under SSP2–4.5 and SSP5–8.5, respectively (see Figure 4d). Late-century projections show stronger warming, with average increases of 3.6°C and 6.8°C under SSP2-4.5 and SSP5-8.5. Summer temperatures (Figure 9e) are projected to increase by 2.2°C and 3.8°C under SSP2–4.5 and SSP5–8.5, respectively, with late-century increases of 2.7°C and 4.8°C. Annual *tas* (Figure 4f) is expected to rise by 2.16°C and 3.32°C under SSP2–4.5 and SSP5–8.5, respectively, with late-century increases of 2.7°C and 5°C. Mid-century changes are smaller than late-century changes. The MME has the lowest uncertainty (inter-model ranges) over the annual, summer and winter timescales. SSP2–4.5 may result in reduced late-century winters and annual timescales. Table 1 indicates significant warming, especially in late-century winter (0.25°C/year) and annual (0.21°C/year) temperatures under SSP5–8.5. Box-whisker plots of *tas* in the 21st century (Figure S20d–f) show significant warming, especially in winters under SSP5–8.5, with a higher median. Zhou et al. (2023) examined annual *tas* projections under SSP2–4.5 (SSP5–8.5) and predicted increases of 1.29°C, 2°C, 2.89°C (1.41°C, 2.52°C, 5.36°C) in the near, mid and long term. Summer temperatures in the QTP region may increase by 1.22°C, 1.88°C, 2.72°C (1.39°C, 2.46°C, 5.01°C) and winter temperatures by 1.42°C, 2.22°C, 3.24°C (1.58°C, 2.77°C, 5.92°C) under SSP2–4.5 (SSP5–8.5).

Figure 6 shows the seasonal and annual spatial distributions of *tas* trends in the 21st century. Winter *tas* (Figure 6a–f) is projected to rise across the QTP, with the northern half experiencing more pronounced warming under both scenarios (0.025°C to 0.040°C/year). Late-century *tas* may warm significantly (0.015°C to 0.040°C/year) under SSP5–8.5 but only slightly (0.004°C to 0.020°C/year) under SSP2–4.5. Summer *tas* (Figure 6g–l) is expected to be much warmer under both scenarios (0.015°C to 0.040°C/year), with late-century summers cooler under SSP2–4.5 compared to mid-century summers. This is reflective of the SSP2–4.5 scenarios' downward trajectory for socioeconomic development and radiative forcing (Gidden et al. 2019). Annual *tas* (Figure 6m–r) is projected to rise (0.016°C to 0.040°C/year) across the QTP. Mid-century years (0.016°C to 0.036°C/year) may experience less warming than late-century years (0.026°C to 0.040°C/year) under SSP5–8.5, while SSP2–4.5 predicts lower warming patterns (0.004°C to 0.032°C/year) for late-century years. Zhang et al. (2023) found that under SSP5–8.5, the *tas* trend over QTP is 0.16°C/decade, with more pronounced effects over the northeastern Plateau. Fan et al. (2022) predict that under SSP5–8.5, northern regions of the TP will see the greatest increases in mean temperature, exceeding 7°C by the end of the 21st century. Late-century *tas* in winters, summers and annual months may show a slight decrease under SSP2–4.5. Winters show stronger warming trends than summers and annual timescales, confirming the persistence of the elevation-dependent warming (EDW) phenomenon. Rangwala et al. (2009) found that western TP warmed more than the eastern TP during the late 20th and early 21st centuries, though the comparisons between warming rates varied significantly with the observation period. Zhou et al. (2023) report that under

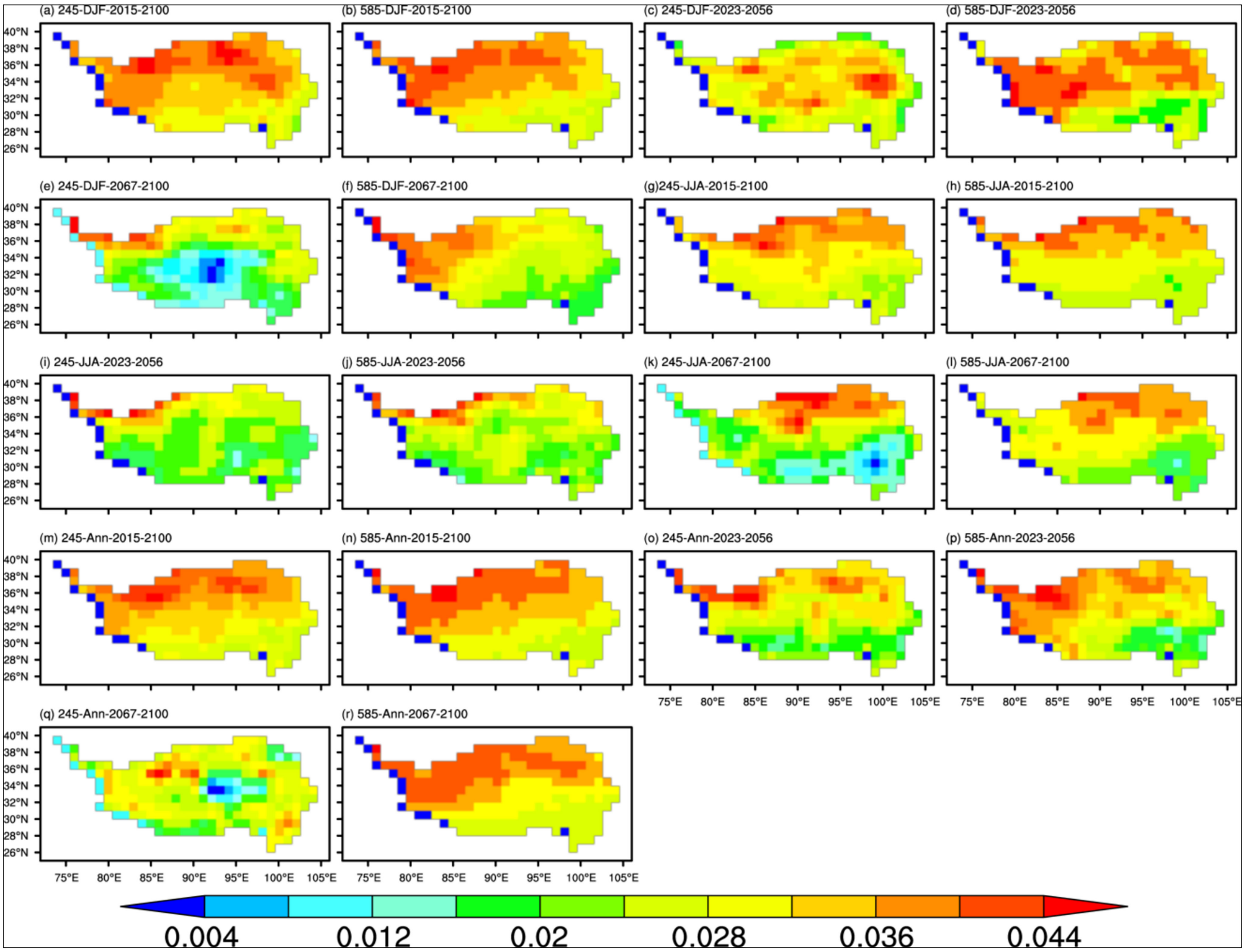

FIGURE 6 | Spatial distribution of projected precipitation variability (standard deviation in mm/day) over the Qinghai–Tibetan Plateau (QTP) under SSP2-4.5 and SSP5-8.5 scenarios for the periods 2015–2100, 2023–2056 and 2067–2100. Panels (a–f) show winter (DJF) variability, (g–l) summer (JJA) variability and (m–r) annual variability. Each row corresponds to a specific time slice, with the left column of each pair representing SSP2-4.5 and the right representing SSP5-8.5. The colour scale indicates the magnitude of interannual variability, ranging from low (blue) to high (red). Results suggest increasing variability across most regions, particularly under SSP5-8.5, with stronger fluctuations in northern and northeastern QTP during winter and in the central and southeastern regions during summer and annually. [Colour figure can be viewed at wileyonlinelibrary.com]

SSP2–4.5 (SSP5–8.5), annual *tas* across the QTP may increase by 0.31°C, 0.29°C, 0.28°C/decade (0.5°C, 0.61°C, 0.74°C/decade). Under SSP2–4.5 (SSP5–8.5), summer temperatures may rise by 0.32°C, 0.31°C, 0.11°C/decade (0.45°C, 0.61°C, 0.68°C/decade). Under SSP2–4.5 (SSP5–8.5), winter temperatures may rise by 0.36°C, 0.36°C, 0.21°C/decade (0.54°C, 0.67°C, 0.83°C/decade).

3.2.3 | Projected Changes in Maximum Temperature (*tmax*)

Projected changes in seasonal and annual *tmax* across the QTP for mid-century (2023–2056) and late-century (2067–2100), relative to 1980–2014, are shown in Figure 7. Winter *tmax* is projected to increase under SSP2-4.5 (2.7°C) and SSP5-8.5 (4.0°C) in mid-century, with late-century warming reaching 3.3°C (SSP2-4.5) and 5.9°C (SSP5-8.5) (Figure 7a). Similarly, summer *tmax* is expected to rise by 2.3°C (SSP2-4.5) and 3.5°C (SSP5-8.5) in mid-century, with further increases of 3.6°C (SSP2-4.5) and 5.9°C (SSP5-8.5) by late-century (Figure 7b). On an annual scale, *tmax* follows a comparable trajectory (Figure 7c), with projected mid-century increases of 2.0°C (SSP2-4.5) and 2.4°C (SSP5-8.5), and late-century warming of 3.2°C (SSP2-4.5) and 5.7°C (SSP5-8.5).

The MME projections show greater uncertainties for *tmax*, particularly during winter, summer and annual timescales. Late-century *tmax* under SSP2-4.5 may exhibit periodic decreases in certain years, suggesting potential interannual variability in warming trends. Table 1 confirms that winter *tmax* warming rates are 0.36°C/decade (SSP2-4.5) and 0.54°C/decade (SSP5-8.5). The annual *tmax* trend is projected at 0.31°C/decade (SSP2-4.5) and 0.5°C/decade (SSP5-8.5). These results are consistent with Zhou et al. (2023), who highlighted that winter and annual temperatures show stronger warming trends compared to summer across the QTP. Box-whisker plots of 21st century *tmax* (Figure S21g–i) show significant warming, especially in winters under SSP5–8.5, with a higher median.

Figure 8 shows the projected rise in *tmax* for winter, summer and annual periods in the 21st century. Under SSP2–4.5 and SSP5–8.5 (0.012°C to 0.040°C/year), winter *tmax* (Figure 8a–f) is expected to warm significantly, particularly at high altitudes on the western QTP. Late-century *tmax* may decrease (0.004°C to 0.028°C/year) over central regions under SSP2–4.5, while mid and late-century *tmax* may rise (0.012°C to 0.040°C/year) under SSP5–8.5. Summer *tmax* (Figure 8g–l) shows significant warming under both scenarios (0.012°C to 0.040°C/year). Under SSP2–4.5, late-century summer *tmax* may show a slower rate of rise over southern parts (0.004°C to 0.028°C/year). Mid and late-century *tmax* under SSP5–8.5 appear significantly higher in the northern QTP. Annual *tmax* (Figure 8m–r) follows similar patterns, with a significant rise (0.02°C to 0.040°C/year) over the northern half of the QTP. Mid and late-century *tmax* under SSP2–4.5 (0.004°C to 0.040°C/year) may show a weaker rise than under SSP5–8.5 (0.012°C to 0.040°C/year). The stronger rise in winter *tmax* at higher altitudes in the western QTP confirms the future phenomenon of EDW.

3.2.4 | Projected Changes in Minimum Temperature (*tmin*)

The *tmin* changes over QTP for 21st century are presented in Figure 7d–f. Winter *tmin* exhibits a stronger warming trend than *tmax* across the QTP. Figure 7d shows that winter *tmin* is projected to rise by 2.4°C (SSP2-4.5) and 2.7°C (SSP5-8.5) in mid-century, with late-century warming reaching 3.6°C (SSP2-4.5) and 6.0°C (SSP5-8.5). Summer *tmin* projections indicate warming of 2.1°C (SSP2-4.5) and 3.3°C (SSP5-8.5) in mid-century, increasing to 2.9°C (SSP2-4.5) and 5.4°C (SSP5-8.5) in late-century (Figure 7e). On an annual scale, *tmin* is expected to increase (Figure 7f) by 1.6°C (SSP2-4.5) and 2.1°C (SSP5-8.5) in mid-century, with late-century warming of 2.9°C (SSP2-4.5) and 5.4°C (SSP5-8.5). Unlike *tmax*, winter *tmin* warming is more substantial across the QTP, consistent with EDW trends. Annual, winter and summer inter-model ranges for *tmin* show a declining trend over the 21st century, suggesting improved model agreement over time. Table 1 confirms that winter *tmin* is projected to rise at a rate of 0.36°C/decade (SSP2-4.5) and 0.67°C/decade (SSP5-8.5), aligning with the findings of Zhou et al. (2023), who reported higher winter warming rates than summer across the QTP. Additionally, box-whisker distributions for winter and annual *tmax* and *tmin* (Figure S21j–l) confirm that *tmin* will warm at a faster rate than *tmax* in mid- and late-century.

Figure 9 shows that winter *tmin* in the 21st century is expected to show stronger warming (0.016°C to 0.044°C/year) across the QTP, especially in the northern parts, similar to the changes in *tmax*. Mid and late-century winters are expected to have a greater rise in *tmin* under SSP5–8.5 (0.012°C–0.044°C/year) than under SSP2–4.5 (0.004°C–0.032°C/year). Summer *tmin* (Figure 9g–l) shows warming tendencies, particularly in the northern parts, under both scenarios (0.012°C to 0.040°C/year). Mid and late-century *tmin* may appear with stronger warming under SSP5–8.5 (0.012°C to 0.040°C/year), while a minor rate of late-century *tmin* rise (0.004°C to 0.028°C/year) is likely over southern QTP under SSP2–4.5. Annual *tmin* (Figure 9m–r) is expected to follow stronger warming tendencies (0.016°C to 0.040°C/year) across the QTP. Southern QTP parts may show a faster increase in *tmin* (0.012°C to 0.040°C/year) under SSP5–8.5 than under SSP2–4.5 (0.004°C to 0.032°C/year). Overall, the 21st century is expected to see a stronger rise in winter *tmin*, followed by annual and summer temperatures across the QTP, particularly at higher altitudes in the western QTP. The future rate of warming in *tmin* on seasonal and annual scales is higher than in *tmax*, confirming that a warming climate may persist in the 21st century.

4 | Discussion

High spatiotemporal changes in precipitation and temperature patterns have an impact on agricultural production, water resources, hydroelectric power generation and the environment in the QTP. GCMs are used to investigate these changes, but their accuracy is limited by biases and uncertainties (You, Jiang, et al. 2016; Hu et al. 2022; Wang et al. 2022). The performance of GCMs is determined by the climate variables used in a given study, and a trade-off must be made between selecting GCMs and obtaining reliable climate projections. Previous research (Cui et al. 2021; Lun et al. 2021; Zhang, Liu, et al. 2022) indicates

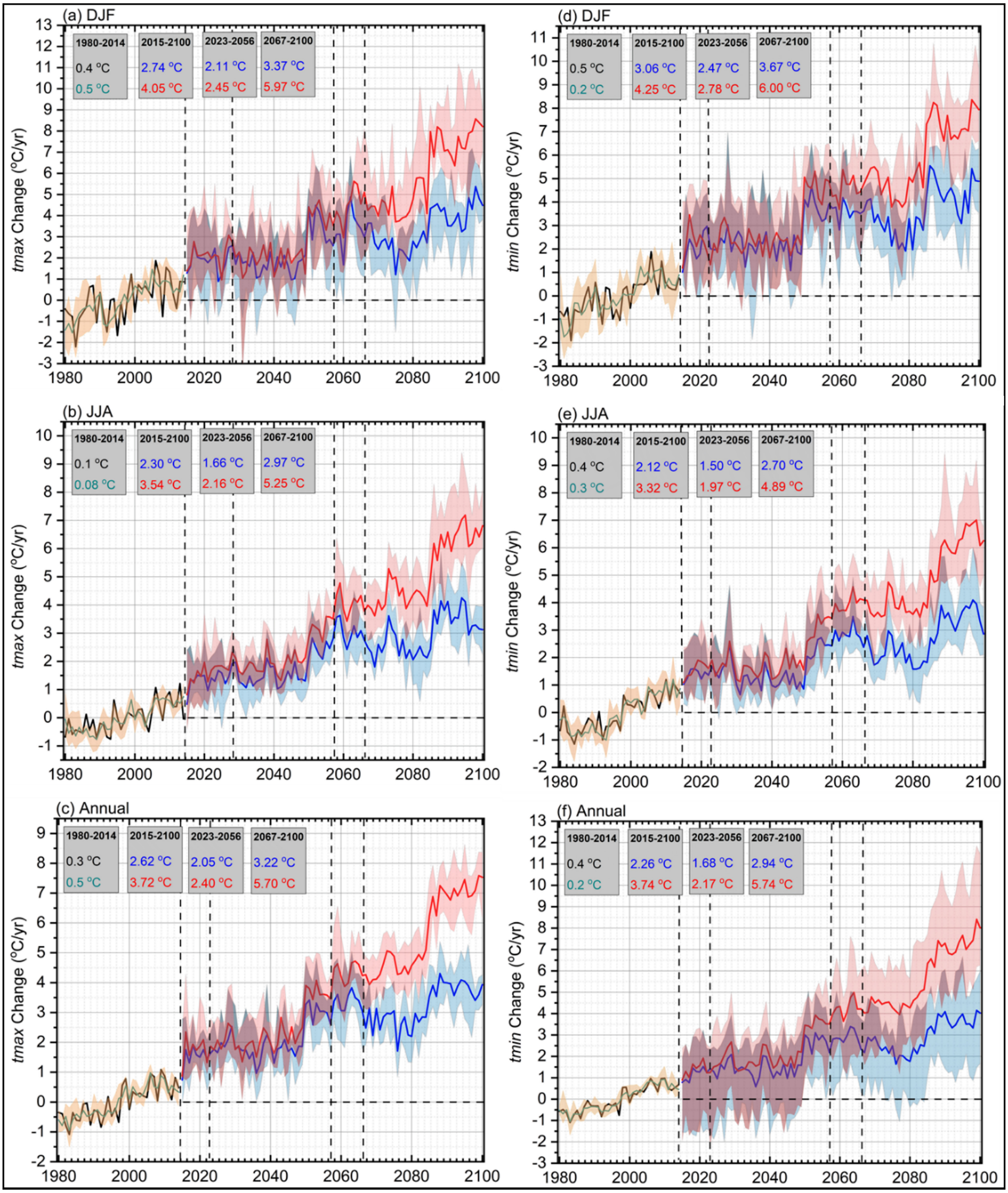

FIGURE 7 | Projections of bias-corrected multi-model ensemble (MME) outputs for seasonal and annual maximum temperature (*tmax*; panels a–c) and minimum temperature (*tmin*; panels d–f) over the Qinghai–Tibetan Plateau (QTP) under SSP2-4.5 (blue line) and SSP5-8.5 (red line), relative to the historical baseline period of 1980–2014 (olive green line). The black solid line represents observed data. Shaded regions indicate the inter-model spread: Orange for historical, light blue for SSP2-4.5 and light red for SSP5-8.5. Vertical dashed lines mark three future time slices: 2015–2100, 2023–2056 and 2067–2100. Mean temperature changes for each period are summarised in grey-shaded boxes, with values shown in green (historical), blue (SSP2-4.5) and red (SSP5-8.5). The projections indicate substantial warming across all scenarios, with stronger increases in *tmin* than *tmax*, particularly under SSP5-8.5 during winter and in the late 21st century. [Colour figure can be viewed at wileyonlinelibrary.com]

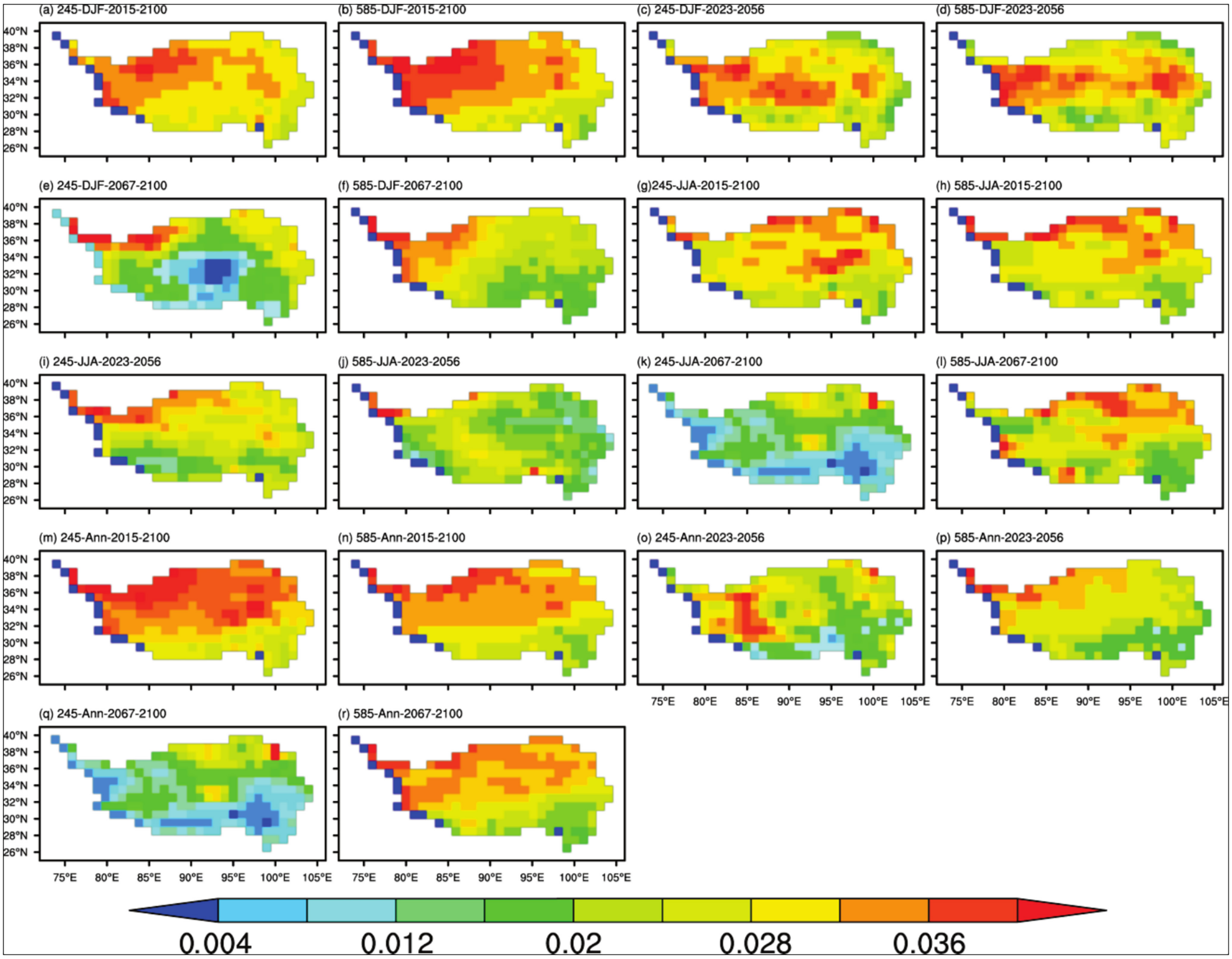

FIGURE 8 | Spatial distribution of projected trends in maximum temperature (*tmax*;°C/year) over the Qinghai–Tibetan Plateau (QTP) under SSP2-4.5 and SSP5-8.5 scenarios for three future periods: 2015–2100, 2023–2056 and 2067–2100. Panels (a–f) represent winter (DJF), (g–l) summer (JJA) and (m–r) annual *tmax* trends. For each pair of panels, the left shows SSP2-4.5 and the right shows SSP5-8.5. The colour scale ranges from low (blue) to high (red) warming rates (°C/year). Results indicate widespread warming across the QTP, with higher trend magnitudes under SSP5-8.5—particularly in the northern and western regions. Winter and annual trends show greater spatial intensity compared to summer, reflecting stronger seasonal warming responses. [Colour figure can be viewed at wileyonlinelibrary.com]

that using suitable GCMs reduces uncertainty in climate variables. The current study proposes intensive evaluation and bias-constrained projections of CMIP6 GCMs for precipitation, *tas*, *tmax* and *tmin* variables in the sensitive region of the QTP.

4.1 | Factors Influencing Precipitation Changes Across QTP

Future projections for precipitation over the QTP show diverse changes. Winter precipitation is expected to increase under SSP2-4.5 and SSP5-8.5, especially in southern to southeastern QTP. Summer and winter precipitation are expected to increase in southeastern QTP, though some parts of northern QTP may experience dry conditions on an annual timescale in mid and late-century under the SSP2-4.5 scenario. Projection works by You, Jiang, et al. (2016), Xu, Guo et al. (2016), Cui et al. (2021), Hu et al. (2022) and Zhang, Liu, et al. (2022) also estimated matching results for precipitation, especially at annual timescales. Chen et al. (2017) revealed that summer precipitation in the QTP will slightly decrease under RCP2.6 by −3.4 mm per decade, while RCP4.5 and RCP8.5 reveal increases by 2.4 and 18.4 mm per decade, respectively. Zhang, Liu, et al. (2022) predicted near-term annual precipitation over QTP from 280 to 660 mm, with mid-term increases of 413–465 mm and 430–465 mm, mainly concentrated in July and August, with 80–90 mm for 2031–2050 and 90–100 mm for 2061–2080. According to Zhou et al. (2023), CMIP6-based estimates of seasonal precipitation accumulations are 218% (spring), 76% (summer), 129% (autumn) and 533% (winter) of those observed. These findings highlight the rise in precipitation changes, yet the factors behind the changes have not been explored.

4.2 | Projected Warming Over the QTP: Trends and Patterns

Our analysis of spatiotemporal surface temperatures (*tas*, *tmax* and *tmin*) from the CMIP6 MME reveals rapid warming

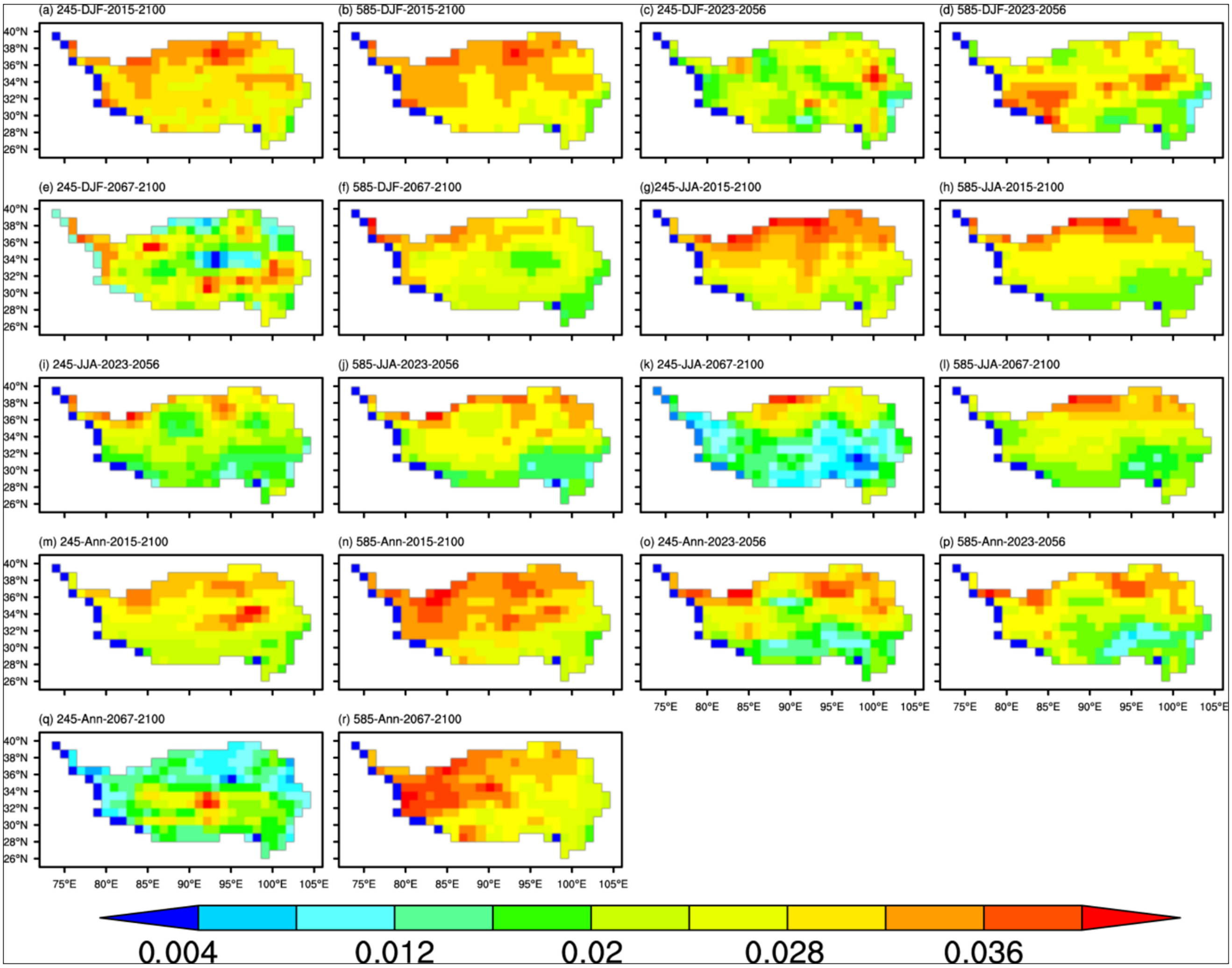

FIGURE 9 | Spatial distribution of projected trends in minimum temperature (*tmin*;°C/year) over the Qinghai–Tibetan Plateau (QTP) under SSP2-4.5 and SSP5-8.5 scenarios for the periods 2015–2100, 2023–2056 and 2067–2100. Panels (a–f) show trends for winter (DJF), (g–l) for summer (JJA) and (m–r) for annual scales. In each panel pair, the left column shows SSP2-4.5 and the right column SSP5-8.5. The colour scale reflects the rate of warming, from lower (blue/green) to higher (yellow/red)°C/year. Results indicate consistent warming in *tmin* across the region, with SSP5-8.5 exhibiting stronger and more spatially extensive trends, particularly during winter and over central and eastern QTP. [Colour figure can be viewed at wileyonlinelibrary.com]

over the QTP in the near, mid and late 21st centuries. Winter *tas*, *tmax* and *tmin* are expected to rise dramatically under higher emission scenarios, particularly in late-century scenarios. Mid- and late-century winter and annual *tas* and *tmin* are expected to warm faster than *tmax*, confirming an asymmetrical warming pattern in which *tmin* rises faster than *tmax*, consistent with Screen's (2014) findings in high latitude regions.

Recent studies highlight an accelerating warming trend across the QTP, with projections under high-emission scenarios exceeding earlier expectations. Zhou and Zhang (2021) found that by the end of the 21st century (2081–2100), projected warming under RCP8.5 and RCP4.5 scenarios is 0.63°C and 0.32°C higher, respectively, than previously estimated. Fan et al. (2022) reported century-scale increases in annual mean temperature reaching 1.25°C, 3.30°C, 5.61°C and 7.46°C under SSP1-2.6, SSP2-4.5, SSP3-7.0 and SSP5-8.5, respectively—highlighting a steep climate gradient tied to emission intensity.

Zhang et al. (2023) reinforced these findings, identifying a robust warming trend under SSP5-8.5, with annual near-surface air temperature (*tas*) rising at a rate of 0.16°C per year. Similarly, Zhou et al. (2023) projected substantial increases in annual *tas* across three future time slices: 1.29°C, 2.00°C and 2.89°C under SSP2-4.5, and 1.41°C, 2.52°C, and 5.36°C under SSP5-8.5. Seasonally, summer warming is expected to reach up to 5.01°C and winter *tas* up to 5.92°C by century's end under SSP5-8.5, indicating intensified warming during the cold season.

Adding to this, Zhang, You, et al. (2022) emphasised the role of EDW, particularly during winter months, with amplified temperature increases over high-altitude regions of the TP. Notably, warming under transient climate scenarios was approximately 0.2°C higher than under stabilised pathways at the same global temperature thresholds—underscoring the importance of emission trajectories in shaping regional climate outcomes.

4.3 | Accelerated Warming Over the QTP: Drivers and Impacts

The accelerated warming over the QTP is driven by interactions such as snow-albedo feedback and cloud-radiation effects (Duan and Xiao 2015; Liu and Chen 2000). Wang et al. (2022) attributed around 60% of the observed warming (1.8°C–2.0°C) from 1980 to 2018 to anthropogenic influences. Temperature variations across the QTP are also linked to elevation differences (Wu et al. 2023) and changes in ENSO episodes, which modify atmospheric circulation anomalies (Yong et al. 2023).

Warming impacts are evident on the QTP, including vegetation degradation, glacier mass loss, permafrost thaw and rising permafrost temperatures (You, Kang, Flügel, et al. 2010; Zhang 2007). Future warming is projected to be influenced by land use changes, atmospheric circulation and surface water vapour, particularly in winter (Song et al. 2021). Additional factors such as cloud cover, ozone and vegetation also play roles (You, Chen, et al. 2020). Guo et al. (2016), Zhou et al. (2023) and You, Chen, et al. (2020) highlight snow-albedo feedbacks and solar radiation as key contributors to EDW over the QTP, leading to increased snow melt and rising snow lines (Yao et al. 2019). Accelerated warming leads to significant changes in hydrology and water resources on and beyond the QTP (Zhou and Zhang 2021; Zhang, Liu, et al. 2022). You, Chen, et al. (2020) reported a west–east gradient in projected snow water equivalent changes, with the largest reductions in the western QTP. The QTP is recognised as a major driver of regional and global environmental changes (You, Kang, Pepin, et al. 2010b).

5 | Conclusion and Recommendations

This study investigates precipitation and air temperature (*tas*, *tmax*, *tmin*) dynamics over the QTP using models from the Coupled Model Intercomparison Project Phase 6 (CMIP6) and high-resolution observational datasets from 1980 to 2100. The research aims to analyse temporal and spatial climate variations, assess GCMs, and provide bias-corrected future projections based on different SSP scenarios.

The results for historical evaluations, detailed in the Supporting Information reveal that the MME significantly overestimates precipitation, with winter observed levels ranging from 0 to 30 mm per year versus MME estimates of 0 to 90 mm. Summer precipitation varies from 240 to 340 mm observed compared to 470 to 520 mm predicted by MME. Annual precipitation is between 440 and 550 mm observed, against MME projections of 960–1065 mm. Temperatures exhibit a warming trend, with annual *tas* increasing by 0.06°C per year, winter temperatures by 0.02°C, and summer by 0.03°C. Winter *tmax* ranges from −4.3°C to 0.1°C observed compared to −7.6 to 5.4°C MME, while winter *tmin* varies from −18.3°C to −15.5°C observed and −18.7°C to −17.1°C MME. The bias analysis shows significant wet biases in southeastern QTP precipitation, with annual biases of 0 to 1100 mm, and summer biases in northern QTP exhibit dry biases of 0 to −100 mm. Temperature biases indicate a cold tendency, especially in central and western areas, with winter biases for *tas* reaching −12°C to 0°C. GCM performance varies significantly, and a bias correction process applied to the top five performing GCMs resulted in improved accuracy for *tas*, *tmax*, *tmin* and precipitation projections.

Future projections indicate a general trend toward warmer and wetter conditions across the QTP, accompanied by significant seasonal and spatial variations. Under the SSP2-4.5 and SSP5-8.5 scenarios, winter precipitation is projected to increase by 2.5 and 10 mm, respectively, with particularly pronounced increases anticipated in the southern and southeastern regions of the QTP. Summer precipitation is expected to rise by 17.4 and 25.3 mm, with the most substantial increases occurring in the southeastern areas of the QTP. Annual precipitation changes may range from a decrease of 2.41 mm to an increase of 6.68 mm, with certain northern regions likely to experience a decline in annual precipitation during the mid to late century under the SSP2-4.5 scenario.

Temperature projections indicate a significant warming trend across the QTP throughout the 21st century, with notable seasonal and spatial variations. Mean winter temperatures (*tas*) are expected to rise by 2.9°C and 4.7°C under the SSP2-4.5 and SSP5-8.5 scenarios, respectively. By the late century, warming could reach between 3.6°C and 6.8°C in the northern and northwestern regions of the QTP. Similarly, summer mean temperatures are projected to increase by 2.2°C and 3.8°C, with projected late-century increases of 2.7°C–4.8°C for northern QTP. Overall, annual mean temperatures are estimated to rise between 2.16°C and 3.32°C, indicating a sustained long-term warming trend under both SSP scenarios.

Projections reveal a consistent and striking asymmetry in warming between minimum (*tmin*) and maximum (*tmax*) temperatures across the QTP. Minimum temperatures are expected to rise more sharply than their daytime counterparts, a pattern most evident during winter. Under SSP2-4.5, winter *tmax* and *tmin* are projected to increase by 2.7°C and 3.1°C, respectively, while under SSP5-8.5, these values rise to 4.0°C and 4.2°C. This disparity is not limited to the cold season—late-century projections suggest that annual and winter *tmin* will continue to outpace *tmax*, reinforcing the asymmetrical warming signal. Summer temperatures follow a similar trajectory, with annual *tmax* and *tmin* expected to increase by 3.72°C and 3.74°C under SSP5-8.5. This persistent amplification of warming may have far-reaching consequences for permafrost stability, hydrological cycles and energy demand, emphasising the need to consider diurnal temperature dynamics in climate impact assessments.

Despite ongoing warming, projections suggest that some central and southern regions of the Tibetan Plateau (QTP) may see a decrease in maximum and minimum temperatures by the late 21st century, indicating regional climate variability. The more significant rise in winter and annual minimum temperatures could have serious implications for ecosystem stability, permafrost degradation and hydrological cycles. These findings highlight the need for further research into regional climate feedbacks and the effects of a changing thermal regime across the QTP.

Projected increases in temperature and precipitation on the QTP could significantly affect water resources, ecosystem stability and the likelihood of natural disasters. Enhanced winter warming may lead to accelerated glacier retreat and permafrost thawing, impacting downstream water availability, while drier conditions in northern regions could heighten drought risks and harm agricultural productivity. To tackle these challenges, collaboration among stakeholders is crucial, focusing on vulnerable areas to improve disaster preparedness, resilience and adaptive strategies, alongside further research into extreme weather events and climate modelling (Shen et al. 2016; Zhang et al. 2019).

Author Contributions

Rizwan Karim: conceptualization, methodology, software, data curation, formal analysis, validation, investigation, visualization, writing – original draft, writing – review and editing, resources, funding acquisition. **Shufeng Li:** conceptualization, methodology, data curation, supervision, project administration, writing – review and editing, funding acquisition. **Tao Su:** conceptualization, methodology, resources, project administration, writing – review and editing. **Brian Odhiambo Ayugi:** conceptualization, methodology, software, data curation, formal analysis, visualization, validation, writing – original draft, writing – review and editing. **Hassen Babaousmail:** software, methodology, formal analysis, visualization, writing – review and editing. **Shumei Xiao:** visualization, writing – review and editing, software, data curation.

Acknowledgements

The authors acknowledge the Xishuangbanna Tropical Botanical Garden–CAS for providing a conducive environment and infrastructural support for conducting research. We are indebted to the World Climate Research Program working group on coupled modelling for making the CMIP models' datasets freely available. We also thank the National Meteorological Information Center, China Meteorological Administration, for providing gridded datasets for the study region.

Disclosure

This study does not include any reproduced or adapted material from other sources. All data used in this research were obtained from publicly available datasets, which are properly cited.

Conflicts of Interest

The authors declare no conflicts of interest.

Data Availability Statement

The data supporting this study's findings are available from the corresponding author upon reasonable request.

References

Ali, S., R. S. Kiani, M. S. Reboita, et al. 2021. "Identifying Hotspots Cities Vulnerable to Climate Change in Pakistan Under CMIP5 Climate Projections." *International Journal of Climatology* 41: 559–581. https://doi.org/10.1002/joc.6638.

Ayugi, B. O., E. S. Chung, H. Babaousmail, and K. T. C. L. K. Sian. 2024. "Characterizing the Performances of Different Observational Precipitation Products and Their Uncertainties Over Africa." *Environmental Research Letters* 19, no. 6: 064009.

Ayugi, B., H. Ngoma, H. Babaousmail, et al. 2021. "Evaluation and Projection of Mean Surface Temperature Using CMIP6 Models Over East Africa." *Journal of African Earth Sciences* 181: 104226. https://doi.org/10.1016/j.jafrearsci.2021.104226.

Ayugi, B., G. Tan, N. Ruoyun, et al. 2020. "Quantile Mapping Bias Correction on Rossby Centre Regional Climate Models for Precipitation Analysis Over Kenya, East Africa." *Water* 12, no. 3: 801. https://doi.org/10.3390/w12030801.

Babaousmail, H., R. Hou, B. Ayugi, et al. 2021. "Evaluation of the Performance of CMIP6 Models in Reproducing Rainfall Patterns Over North Africa." *Atmosphere* 12: 475. https://doi.org/10.3390/atmos12040475.

Brunner, L., A. Pendergrass, F. Lehner, et al. 2020. "Reduced Global Warming From CMIP6 Projections When Weighting Models by Performance and Independence." *Earth System Dynamics Discussions* 6: 1–23. https://doi.org/10.5194/esd-2020-23.

Cardell, M. F., R. Romero, A. Amengual, V. Homar, and C. Ramis. 2019. "A Quantile–Quantile Adjustment of the EURO-CORDEX Projections for Temperatures and Precipitation." *International Journal of Climatology* 39: 2901–2918. https://doi.org/10.1002/joc.5991.

Chen, F., J. Zhang, J. Liu, et al. 2020. "Climate Change, Vegetation History, and Landscape Responses on the Tibetan Plateau during the Holocene: A Comprehensive Review." *Quaternary Science Reviews* 243: 106444. https://doi.org/10.1016/j.quascirev.2020.106444.

Chen, X., Q. You, F. Sielmann, and N. Ruan. 2017. "Climate Change Scenarios for Tibetan Plateau Summer Precipitation Based on Canonical Correlation Analysis." *International Journal of Climatology* 37: 1310–1321. https://doi.org/10.1002/joc.4778.

Cui, T., C. Li, and F. Tian. 2021. "Evaluation of Temperature and Precipitation Simulations in CMIP6 Models Over the Tibetan Plateau." *Earth and Space Science* 8: 1–20. https://doi.org/10.1029/2020EA001620.

Duan, A., and Z. Xiao. 2015. "Does the Climate Warming Hiatus Exist Over the Tibetan Plateau?" *Scientific Reports* 5: 13711. https://doi.org/10.1038/srep13711.

Fan, X., Q. Duan, C. Shen, Y. Wu, and C. Xing. 2022. "Evaluation of Historical CMIP6 Model Simulations and Future Projections of Temperature Over the Pan-Third Pole Region." *Environmental Science and Pollution Research* 29: 26214–26229. https://doi.org/10.1007/s11356-021-17474-7.

Farooqui, M. N. I., and G. Y. Soomro. 1984. "An Analysis of Fertility Change in Pakistan." *Pakistan Development Review* 23: 225–238.

Feng, W., H. Lu, T. Yao, and Q. Yu. 2020. "Drought Characteristics and Its Elevation Dependence in the Qinghai–Tibet Plateau During the Last Half-Century." *Scientific Reports* 10: 14323. https://doi.org/10.1038/s41598-020-71295-1.

Gidden, M. J., K. Riahi, S. J. Smith, et al. 2019. "Global Emissions Pathways Under Different Socioeconomic Scenarios for Use in CMIP6: A Dataset of Harmonized Emissions Trajectories Through the End of the Century." *Geoscientific Model Development* 12: 1443–1475. https://doi.org/10.5194/gmd-12-1443-2019.

Gudmundsson, L., J. B. Bremnes, J. E. Haugen, and T. Engen-Skaugen. 2012. "Downscaling RCM Precipitation to the Station Scale Using Quantile Mapping—A Comparison of Methods." *Hydrology and Earth System Sciences* 16, no. 9: 3383–3390. https://doi.org/10.5194/hess-16-3383-2012.

Guo, D., E. Yu, and H. Wang. 2016. "Will the Tibetan Plateau Warming Depend on Elevation in the Future?" *Journal of Geophysical Research* 121: 3969–3978. https://doi.org/10.1002/2016JD024871.

Gupta, R., R. Bhattarai, and A. Mishra. 2019. "Development of Climate Data Bias Corrector (CDBC) Tool and Its Application over the Agro-Ecological Zones of India." *Water* 11, no. 5: 1102. https://doi.org/10.3390/w11051102.

Haigh, J. D. 1996. "The Impact of Solar Variability on Climate." *Science* 272: 981–984. https://doi.org/10.1126/science.272.5264.981.

Hawkins, E., P. Ortega, E. Suckling, et al. 2020. "Estimating Changes in Global Temperature Since the Preindustrial Period." *Bulletin of the American Meteorological Society* 101, no. 11: E1942–E1956. https://doi.org/10.1175/BAMS-D-19-0033.1.

Hu, Q., D. Jiang, and G. Fan. 2014. "Evaluation of CMIP5 Models Over the Qinghai–Tibetan Plateau." *Chinese Journal of Atmospheric Sciences* 38: 924–938.

Hu, W., L. Chen, J. Shen, J. Yao, Q. He, and J. Chen. 2022. "Changes in Extreme Precipitation on the Tibetan Plateau and Its Surroundings: Trends, Patterns, and Relationship With Ocean Oscillation Factors." *Water* 14, no. 16: 2509. https://doi.org/10.3390/w14162509.

Iyakaremye, V., G. Zeng, A. Siebert, and X. Yang. 2021. "Contribution of External Forcings to the Observed Trend in Surface Temperature Over Africa During 1901–2014 and Its Future Projection From CMIP6 Simulations." *Atmospheric Research* 254: 105512. https://doi.org/10.1016/j.atmosres.2021.105512.

Jiang, D., H. Wang, and X. Lang. 2005. "Evaluation of East Asian Climatology as Simulated by Seven Coupled Models." *Advances in Atmospheric Sciences* 22: 479–495. https://doi.org/10.1007/bf02918482.

Jiang, D., Z. Tian, and X. Lang. 2016. "Reliability of Climate Models for China Through the IPCC Third to Fifth Assessment Reports." *International Journal of Climatology* 36: 1114–1133. https://doi.org/10.1002/joc.4406.

Jose, D. M., and G. S. Dwarakish. 2022. "Bias Correction and Trend Analysis of Temperature Data by a High-Resolution CMIP6 Model Over a Tropical River Basin." *Asia-Pacific Journal of Atmospheric Sciences* 58: 97–115. https://doi.org/10.1007/s13143-021-00240-7.

Karim, R., G. Tan, B. Ayugi, et al. 2023. "Projected Changes in Surface Air Temperature Over Pakistan Under Bias-Constrained CMIP6 Models." *Arabian Journal of Geosciences* 16: 205. https://doi.org/10.1007/s12517-023-11243-1.

Karim, R., G. Tan, B. Ayugi, H. Babaousmail, and F. Liu. 2020. "Evaluation of Historical CMIP6 Model Simulations of Seasonal Mean Temperature Over Pakistan During 1970-2014." *Atmosphere (Basel)* 11: 1005. https://doi.org/10.3390/atmos11091005.

Kendall, M. G. 1975. *Rank Correlation Methods*. 4th ed. Charles Griffin.

Kuang, X., and J. J. Jiao. 2016. "Review on Climate Change on the Tibetan Plateau During the Last Half-Century." *Journal of Geophysical Research* 121: 3979–4007. https://doi.org/10.1002/2015JD024728.

Li, X., L. Wang, X. Guo, and D. Chen. 2017. "Does Summer Precipitation Trend Over and Around the Tibetan Plateau Depend on Elevation?" *International Journal of Climatology* 37: 1278–1284. https://doi.org/10.1002/joc.4978.

Liu, X., and B. Chen. 2000. "Climatic Warming in the Tibetan Plateau During Recent Decades." *International Journal of Climatology* 20: 1729–1742. https://doi.org/10.1002/1097-0088(20001130)20:14<1729::AID-JOC556>3.0.CO;2-Y.

Lu, K., M. Arshad, X. Ma, I. Ullah, J. Wang, and W. Shao. 2022. "Evaluating Observed and Future Spatiotemporal Changes in Precipitation and Temperature Across China Based on CMIP6-GCMs." *International Journal of Climatology* 42, no. 15: 7703–7729. https://doi.org/10.1002/joc.7673.

Lun, Y., L. Liu, L. Cheng, X. Li, H. Li, and Z. Xu. 2021. "Assessment of GCMs Simulation Performance for Precipitation and Temperature From CMIP5 to CMIP6 Over the Tibetan Plateau." *International Journal of Climatology* 41: 3994–4018. https://doi.org/10.1002/joc.7055.

Maher, N., D. Matei, S. Milinski, and J. Marotzke. 2018. "ENSO Change in Climate Projections: Forced Response or Internal Variability?" *Geophysical Research Letters* 45, no. 20. https://doi.org/10.1029/2018gl079764.

Mann, H. B. 1945. "Nonparametric Tests Against Trend." *Econometrica* 13: 245. https://doi.org/10.2307/1907187.

Maraun, D. 2013. "Bias Correction, Quantile Mapping, and Downscaling: Revisiting the Inflation Issue." *Journal of Climate* 26, no. 6: 2137–2143. https://doi.org/10.1175/JCLI-D-12-00821.1.

Meehl, G. A., J. M. Arblaster, and G. Branstator. 2008. "A Coupled Air-Sea Response Mechanism to Solar Forcing in the Pacific Region." *Journal of Climate* 21: 2883–2897. https://doi.org/10.1175/2007JCLI1776.1.

Milinski, S., N. Maher, and D. Olonscheck. 2019. "How Large Does a Large Ensemble Need to Be?" *Geophysical Research Letters* 46: 9123–9132. https://doi.org/10.1029/2019GL083946.

Ngoma, H., W. Wen, B. Ayugi, H. Babaousmail, R. Karim, and V. Ongoma. 2021. "Evaluation of Precipitation Simulations in CMIP6 Models Over Uganda." *International Journal of Climatology* 41, no. 9: 4743–4768. Portico. https://doi.org/10.1002/joc.7098.

Rangwala, I., J. R. Miller, G. L. Russell, and M. Xu. 2009. "Using a Global Climate Model to Evaluate the Influences of Water Vapor, Snow Cover and Atmospheric Aerosol on Warming in the Tibetan Plateau During the Twenty-First Century." *Climate Dynamics* 34, no. 6: 859–872. https://doi.org/10.1007/s00382-009-0564-1.

Screen, J. A. 2014. "Arctic Amplification Decreases Temperature Variance in Northern Mid- to High-Latitudes." *Nature Climate Change* 4, no. 7: 577–582. https://doi.org/10.1038/nclimate2268.

Shen, M., S. Piao, X. Chen, et al. 2016. "Strong Impacts of Daily Minimum Temperature on the Green-Up Date and Summer Greenness of the Tibetan Plateau." *Global Change Biology* 22, no. 9: 3057–3066. Portico. https://doi.org/10.1111/gcb.13301.

Song, X., D.-Y. Wang, F. Li, and X.-D. Zeng. 2021. "Evaluating the Performance of CMIP6 Earth System Models in Simulating Global Vegetation Structure and Distribution." *Advances in Climate Change Research* 12, no. 4: 584–595. https://doi.org/10.1016/j.accre.2021.06.008.

Taylor, K. E. 2001. "Summarizing Multiple Aspects of Model Performance in a Single Diagram." *Journal of Geophysical Research: Atmospheres* 106, no. D7: 7183–7192. Portico. https://doi.org/10.1029/2000jd900719.

Ullah, I., F. Saleem, V. Iyakaremye, et al. 2022. "Projected Changes in Socioeconomic Exposure to Heatwaves in South Asia Under Changing Climate." *Earth's Future* 10, no. 2: e2021EF002240. https://doi.org/10.1029/2021EF002240.

Wang, Y., P. Yan, F. Ji, B. Huang, P. Fan, and G. Feng. 2022. "Anthropogenic Contribution to the Rapid Warming over the Tibetan Plateau." *Climate Dynamics* 61, no. 1–2: 329–339. https://doi.org/10.1007/s00382-022-06576-8.

Wu, J., and G. Xue-Jie. 2013. "A Gridded Daily Observation Dataset Over China Region and Comparison With the Other Datasets." *Chinese Journal of Geophysics* 56, no. 4: 1102–1111. https://doi.org/10.6038/cjg20130406.

Wu, F., Q. You, Z. Cai, G. Sun, I. Normatov, and S. Shrestha. 2023. "Significant Elevation Dependent Warming Over the Tibetan Plateau After Removing Longitude and Latitude Factors." *Atmospheric Research* 284: 106603. https://doi.org/10.1016/j.atmosres.2022.106603.

Xu, J., Y. Gao, D. Chen, L. Xiao, and T. Ou. 2016. "Evaluation of Global Climate Models for Downscaling Applications Centred Over the Tibetan Plateau." *International Journal of Climatology* 37, no. 2: 657–671. https://doi.org/10.1002/joc.4731.

Xu, X., Z. Zhang, and Q. Wu. 2016. "Simulation of Permafrost Changes on the Qinghai–Tibet Plateau, China, Over the Past Three Decades." *International Journal of Digital Earth* 10, no. 5: 522–538. https://doi.org/10.1080/17538947.2016.1237571.

Xu, Z. X., T. L. Gong, and J. Y. Li. 2007. "Decadal Trend of Climate in the Tibetan Plateau—Regional Temperature and Precipitation." *Hydrological Processes* 22, no. 16: 3056–3065. https://doi.org/10.1002/hyp.6892.

Yao, T., Y. Xue, D. Chen, et al. 2019. "Recent Third Pole's Rapid Warming Accompanies Cryospheric Melt and Water Cycle Intensification and Interactions Between Monsoon and Environment: Multidisciplinary Approach With Observations, Modeling, and Analysis." *Bulletin of the American Meteorological Society* 100: 423–444. https://doi.org/10.1175/BAMS-D-17-0057.1.

Yong, Z., Z. Wang, J. Xiong, C. Ye, H. Sun, and S. Wu. 2023. "Variability in Temperature Extremes Across the Tibetan Plateau and Its

Non-Uniform Responses to Different ENSO Types." *Climatic Change* 176: 91. https://doi.org/10.1007/s10584-023-03566-5.

You, Q., D. Chen, F. Wu, et al. 2020. "Elevation-Dependent Warming Over the Tibetan Plateau: Patterns, Mechanisms, and Perspectives." *Earth-Science Reviews* 210: 103349. https://doi.org/10.1016/j.earscirev.2020.103349.

You, Q., D. Wang, Z. Jiang, and S. Kang. 2017. "Diurnal Temperature Range in CMIP5 Models and Observations on the Tibetan Plateau." *Quarterly Journal of the Royal Meteorological Society* 143: 1978–1989. https://doi.org/10.1002/qj.3057.

You, Q., S. Kang, N. Pepin, et al. 2010b. "Relationship Between Temperature Trend Magnitude, Elevation, and Mean Temperature in the Tibetan Plateau From Homogenized Surface Stations and Reanalysis Data." *Global and Planetary Change* 71: 124–133. https://doi.org/10.1016/j.gloplacha.2010.01.020.

You, Q., S. Kang, W. A. Flügel, et al. 2010. "From Brightening to Dimming in Sunshine Duration Over the Eastern and Central Tibetan Plateau (1961–2005)." *Theoretical and Applied Climatology* 101: 445–457. https://doi.org/10.1007/s00704-009-0231-9.

You, Q., Y. Bao, Z. Jiang, N. Pepin, and G. W. K. Moore. 2019. "Surface Pressure and Elevation Correction From Observation and Multiple Reanalyses Over the Tibetan Plateau." *Climate Dynamics* 53: 5893–5908. https://doi.org/10.1007/s00382-019-04905-y.

You, Q., Z. Cai, F. Wu, Z. Jiang, N. Pepin, and S. S. P. Shen. 2021. "Temperature Dataset of CMIP6 Models Over China: Evaluation, Trend and Uncertainty." *Climate Dynamics* 57: 17–35. https://doi.org/10.1007/S00382-021-05691-2.

You, Q., Z. Jiang, Y. Bao, N. Pepin, and K. Fraedrich. 2016. "Trends in Upper Tropospheric Water Vapour Over the Tibetan Plateau From Remote Sensing." *International Journal of Climatology* 36: 4862–4872. https://doi.org/10.1002/joc.4674.

Zhang, Y., L. Bingyuan, L. Linshan, and D. Zheng. 2021. "Redetermine the Region and Boundaries of Tibetan Plateau." *Geographical Research* 40, no. 6: 1543–1553. https://doi.org/10.11821/dlyj020210138.

Zhang, J., Q. You, F. Wu, Z. Cai, and N. Pepin. 2022. "The Warming of the Tibetan Plateau in Response to Transient and Stabilized 2.0°C/1.5°C Global Warming Targets." *Advances in Atmospheric Sciences* 39: 1198–1206. https://doi.org/10.1007/s00376-022-1299-8.

Zhang, J., T. Wu, X. Xin, et al. 2023. "Surface Air Temperature Trend Over the Tibetan Plateau in CMIP6 and Its Constraint in Future Projection." *Journal of Geophysical Research: Atmospheres* 128, no. 21. https://doi.org/10.1029/2023jd039527.

Zhang, Q., K. Fan, V. P. Singh, C. Song, C. Y. Xu, and P. Sun. 2019. "Is Himalayan-Tibetan Plateau "Drying"? Historical Estimations and Future Trends of Surface Soil Moisture." *Science of the Total Environment* 658: 374–384. https://doi.org/10.1016/j.scitotenv.2018.12.209.

Zhang, T. 2007. "Perspectives on Environmental Study of Response to Climatic and Land Cover/Land Use Change Over the Qinghai-Tibetan Plateau: An Introduction." *Arctic, Antarctic, and Alpine Research* 39: 631–634. https://doi.org/10.1657/1523-0430(07-513)[ZHANG]2.0.CO;2.

Zhang, W., L. Liu, Y. Lun, L. Cheng, X. Li, and Z. Xu. 2022. "Projections of Future Precipitation and Air Temperature Over the Tibetan Plateau Based on Coupled Model Intercomparison Project Phase 6 Multimodel Ensembles." *International Journal of Climatology* 42: 9788–9822. https://doi.org/10.1002/joc.7865.

Zhou, M., Z. Yu, H. Gu, et al. 2023. "Evaluation and Projections of Surface Air Temperature Over the Tibetan Plateau From CMIP6 and CMIP5: Warming Trend and Uncertainty." *Climate Dynamics* 60: 3863–3883. https://doi.org/10.1007/s00382-022-06518-4.

Zhou, T., and W. Zhang. 2021. "Anthropogenic Warming of Tibetan Plateau and Constrained Future Projection." *Environmental Research Letters* 16: 044039. https://doi.org/10.1088/1748-9326/abede8.

Supporting Information

Additional supporting information can be found online in the Supporting Information section.